



## Microstructure-sensitive investigation of magnesium alloy fatigue



K. Hazeli<sup>a</sup>, H. Askari<sup>b</sup>, J. Cuadra<sup>a</sup>, F. Streller<sup>c</sup>, R.W. Carpick<sup>d</sup>, H.M. Zbib<sup>b</sup>, A. Kontsos<sup>a,\*</sup>

<sup>a</sup> Department of Mechanical Engineering & Mechanics, Drexel University, USA

<sup>b</sup> School of Mechanical and Materials Engineering, Washington State University, USA

<sup>c</sup> Department of Materials Science & Engineering, University of Pennsylvania, USA

<sup>d</sup> Department of Mechanical Engineering & Applied Mechanics, University of Pennsylvania, USA

### ARTICLE INFO

#### Article history:

Received 25 May 2014

Received in final revised form 7 October 2014

Available online 1 November 2014

#### Keywords:

A. Fatigue

A. Twinning

B. Polycrystalline material

B. Crystal plasticity

C. Nondestructive evaluation

### ABSTRACT

This article presents results relating macroscopic fatigue behavior to microplasticity, twinning activity, and early fatigue crack formation in wrought magnesium alloy specimens of the AZ series. Experimental data were obtained by testing standard-sized samples prepared to be also suitable for direct microstructural quantification using scanning electron microscopy and electron back scatter diffraction for texture, grain-scale observations and fractography, as well as surface morphology measurements using white-light interferometry. In addition, *in situ* nondestructive monitoring of the fatigue behavior was performed by using the Acoustic Emission method. To describe the plastic anisotropy, tension-compression asymmetry, pseudoelasticity and their evolution as a function of fatigue loading, strain-control experiments of varying amplitude were conducted in several steps. Experimental measurements at different stages of fatigue life revealed repeatable occurrences of twinning–detwinning, which is further shown to be coupled with reversible surface roughening. It was also found that although tension twinning contributes considerably to overall plasticity, it could also give rise to crack initiation towards the end of the fatigue life. The role of the reported microplasticity effects was additionally explored using a Continuum Dislocation Dynamics Viscoplastic Self-Consistent (CDD-VPSC) model for the first two cycles of the fatigue life. The intention of this section was to incorporate the effect of twinning–detwinning into the CDD-VPSC model and subsequently to capture the experimental effects associated with changes in the fatigue hysteresis observed between first and second cycle. These simulation results were consistent with the hypothesis that detwinning is responsible for the anomalous hardening behavior during the tensile part of the cyclic loading in the first few cycles of loading. This observation was confirmed for several imposed strain amplitudes and was achieved by properly defining an appropriate boundary condition that allows surface morphology changes. Furthermore, the experimental test plan allowed the quantification of the fatigue life in terms of hysteresis loop parameters including plastic/elastic energy, residual stiffness, as well as mean and extreme stresses. Finally, an energy-based relationship for the evaluation of fatigue behavior based on the Ellyin–Kujawski formulation was found to provide life predictions that agree with obtained experimental information.

© 2014 Elsevier Ltd. All rights reserved.

\* Corresponding author. Tel.: +1 215 895 2297.

E-mail address: [akontsos@coe.drexel.edu](mailto:akontsos@coe.drexel.edu) (A. Kontsos).

## 1. Introduction

Processing improvements of Mg alloys, for example cold forming, depend on understanding microstructure–property–behavior linkages capable of accurately describing plastic deformation and damage initiation (Al-Maharbi et al., 2011; Barnett et al., 2004). Although significant progress in this direction has been made (Agnew and Duygulu, 2005; Begum et al., 2009; Fan et al., 2009; Hasegawa et al., 2007; Ishihara et al., 2007; Koike et al., 2010; Lv et al., 2009; Matsuzuki and Horibe, 2009; Wu et al., 2008a, 2010, 2008c; Yang et al., 2011, 2008; Yin et al., 2008a), there is a noticeable gap in relating microstructure, plasticity and fatigue crack initiation in Mg alloys which is crucial in a materials-by-design context.

Although the effect of microstructural features on the fatigue behavior of polycrystalline materials was documented since the early 1900s (Ewing and Humfrey, 1903), a microstructure-related mechanics framework for quantitative modeling of fatigue failure has not yet been developed (McDowell, 2007; McDowell and Dunne, 2010). Microstructures consist of features at length scales ranging from nanometers to several hundred micrometers with complex geometries and varied orientations. Consequently, several spatial correlations and interactions, especially under cyclic loading may occur, which significantly increase the difficulties associated with both experimental and modeling approaches for physics-based understanding of plasticity and fatigue. This article presents experimental and computational results based on the premise that fatigue and related damage incubation/initiation are complex evolutionary processes, which are highly dependent on hierarchical microstructural evolution (McDowell, 2007; Shan and Gokhale, 2004) and are driven by localized plasticity effects. Several studies attempted to develop a constitutive model based on descriptions of the microstructure evolution and its relationship with internal stress variables (Brahme et al., 2011; Pham et al., 2013). For example, it is shown that the most significant effect of back stress is the selective increase in activity on some slip system and reduction of slip system activity on other slip systems in FCC metals. This observation is supported by the thinning and alignment of slip bands along preferred crystallographic directions (Brahme et al., 2011). Pham et al. (2013) studied intergranular back stress associated with the long-range interaction of dislocations which arises due to the grain-to-grain strain incompatibility in austenitic stainless steel. This study reports that the back stress evolves with the development of boundary and interior dislocations in the beginning, and with grain fragmentation upon further cyclic loading. The effect of microscopic features on macroscopic strain rate sensitivity has been also noted in the literature (Kabirian et al., 2014; Wei et al., 2004). Stress fields associated with migrated atoms cause a drag force on mobile dislocations in FCC structures (Kabirian et al., 2014). The longer the stoppage time, the larger the solute atoms cluster and its associated drag force, so the mobile dislocations, in turn, require more applied force to overcome this barrier.

Wu et al. (2008a) studied the internal stress (strain) evolution during cyclic deformation in Mg ZK40 using *in situ* neutron diffraction and found it to be dominated by tension twinning and detwinning. These authors further showed that grains that undergo twinning, are relaxed relative to its neighbors. This load redistribution between soft and hard grain orientations is attributable to plastic anisotropy. Texture evolution has been also suggested to play a role in plastic anisotropy. In-plane plastic anisotropy of Mg AZ31 for example was attributed to the initial texture (John Neil and Agnew, 2009) while it was further reported that non-basal cross-slip of  $\langle a \rangle$ -type dislocations was greater than anticipated (Agnew and Duygulu, 2005). In addition, Oppedal and coworkers (Oppedal et al., 2012) recently investigate hardening mechanisms in pure Mg and proposed a dislocation-based formalism to model plastic anisotropy.

The effect of local microstructure on macroscopically observed fatigue behavior has been researched in the literature. For instance, analysis of the cyclic stress–strain response and the evolution of fatigue hysteresis shape showed that the back stress component of the cyclic stress is significantly affected by grain size (Morrison and Moosbrugger, 1997). Furthermore, the difference in cyclic plasticity behavior between two samples with different grain sizes has been related to the effect of grain size on Persistent Slip Band (PSB) morphology. Note that the PSBs are generally characterized as regions of localized deformation arising from intense dislocation activity (Venkataraman et al., 1991). In addition, Zhang and Jiang (2006) concluded that the fatigue stress–strain response of polycrystalline copper is a strong function of the grain size and texture.

Fatigue crack initiation has been shown to be highly dependent on the degree of strain localization, which in turn depends on both microstructure and active deformation modes (Antolovich and Armstrong, 2014). Within this framework, several studies reported that a fatigue crack is formed as the result of localized plastic deformation during cyclic straining (Chan, 2010; Finney and Laird, 1975; Harvey et al., 1994; Peralta et al., 2007; Ritchie and Suresh, 1982). In these investigations, evidences are provided on the fact that cracks nucleation could occur under cyclic straining due to the formation of irreversible slip bands. Finney and Laird (1975) stated that a heavy concentration of strain within PSB structures produces a soft region compared to other regions. This observation is generally referred to as “ductility exhaustion”. Basinski et al. (1983) further reported gradually increasing PSB intensity as a function of fatigue cycles in copper single crystal. In their study, it appeared that the PSBs begin when the cyclic hardening curve reaches its maximum, while they multiply rapidly and increase in width as the stress–strain curve show pronounced softening. In order to develop a stress–life relation, Tanaka and Mura (1982) considered material responses related to the extrusion–intrusion mechanism produced by PSBs, whose coalescences ultimately lead to crack nucleation. This observation is mostly applicable to FCC metals, however, tension–compression asymmetry is usually negligible in this type of materials.

Crack initiation is, in general, highly dependent upon the degree of localization of processes which themselves are closely related to microstructure and texture. Localized strain, for example, promotes early crack initiation because the macroscopically imposed strain must be carried in relatively few active regions (Antolovich and Armstrong, 2014; Wang et al., 2011). It has been shown that Portevin–Le Chatelier (PLC) instabilities result in strain bursts in the form of bands that have been suggested to play a crucial role in crack initiation (Wang et al., 2011). Local deformation heterogeneities induced by the microstructure have been also reported to influence fatigue crack initiation and micro-crack propagation (Abuzaid et al., 2013). Abuzaid et al. additionally describe necessary conditions and precursors for fatigue crack nucleation in polycrystal Hastelloy. Investigation of the fatigue behavior of  $\alpha$ -iron polycrystal at a high cyclic strain rate revealed the development of surface roughening with periodicity comparable to the grain size, which lead to fatigue crack initiation (Mughrabi et al., 1981). In addition, an elaborate study by Man et al. (2012) demonstrated that cyclic strain localization leads to PSBs with specific dislocation structure, followed by distinctive surface slip marks (surface extrusion and intrusion) which further promote fatigue cracking. Besides intrusions and extrusions, fatigue crack initiation may occur at grain or twin boundaries as the result of slip impingement (Chan, 2010).

In the case of Mg, since the grain boundaries are sufficiently strong (Koike, 2005), additional stresses arise to maintain strain compatibility, which can cause the activation of twinning and non-basal slip. It is, however, possible that stress (strain) concentrations due to incompatibilities between twins and their surrounding matrix regions to be relaxed by slip (Ando et al., 2010; Vaidya and Mahajan, 1980) or crack formation (Yoo, 1981). This type of complex local plasticity becomes even more complicated when twinning–detwinning interchange. Cyclic experiments on HCP materials such as Mg are typically more complex compared to other metals due to their dependence on both strong twinning (Khan et al., 2011; Lou et al., 2007; Zeng et al., 2010) and texture effects (Barnett, 2001; Hazeli et al., 2013a). For instance, the relative prevalence of certain deformation mechanisms in Mg alloys subjected to cyclic loading strongly depends on both the initial and the evolving texture. Consequently, the measured compressive yield stress is significantly less than the corresponding tensile. In addition, although basal slip and twinning are mostly activated during compression, in reversed loading the hardening behavior further involves detwinning as well as harder slip systems, including pyramidal and/or prismatic (Wu et al., 2010; Wu et al., 2008c). In general, studies on the specific influence of texture on the cyclic response of polycrystals are scarce (Chan, 2010; Le Biavant et al., 2002; Llanes et al., 1993). For example, Chan (2010) showed that texture may enhance fatigue crack initiation if groups of grains are oriented favorably for slip. In highly textured Mg alloys,  $\{10\bar{1}2\}$  tension twinning was found to primarily form during the compressive part of cyclic loading (Park et al., 2010a). In materials that twin considerably, twinning and its interaction with slip can result in a Bauschinger-like effect (Karaman et al., 2001). Local stress states during plastic deformation of Mg alloys at room temperature greatly depend on twinning (Barnett et al., 2012; Hazeli et al., 2013a; Muránsky et al., 2010), which also eventually drives the associated microstructure evolution (Jiang et al., 2007) and has been also recently incorporated into computational models (Lou et al., 2007; Wang et al., 2013).

In agreement with Barnett et al. (2012), the authors recently demonstrated (Hazeli et al., 2013a) that the near yielding behavior is dominated by twin-related strain localizations that form characteristic and macroscopically-observed band-like structures. Twins were found to propagate from grain to grain, starting from grains with orientations closer to the basal plane (Hazeli et al., 2013b; Lou et al., 2007). It has been suggested that this effect leads to stress relaxation at the tip of growing twins (Ando et al., 2010; Barnett et al., 2012). A previous study by Partridge (1965) shows that twins can disappear or become narrower under reverse loading. *In situ* bending experiments coupled with Nomarsky interference contrast in fact showed that detwinning is possible to occur when the applied load decreases (Caceres et al., 2003). Combinations of axial–torsion loading further showed that the occurrence of twinning and detwinning resulted in asymmetric shear stress–shear strain hysteresis loops (Zhang et al., 2011). Despite the aforementioned references to twinning–detwinning and its subsequent effects on tension–compression asymmetry and also on strain hardening rate (Begum et al., 2009; Hyuk Park et al., 2010; Lou et al., 2007; Lugo et al., 2013; Lv et al., 2011; Matsuzuki and Horibe, 2009), there are still some fundamental questions to be answered. Specifically, the direct evidence of the role of twinning–detwinning in fatigue damage initiation is scarce in the relevant literature (Yang et al., 2011). Furthermore, to the authors' best knowledge, the evolution of surface roughness during fatigue loading has not been investigated and associated with evolutionary fatigue incubation conditions, as shown in this article.

The results presented in this article suggest that the role of strain localization becomes more pronounced in the case of HCP metals. It is widely accepted that deformation twinning offers options for plastic flow accommodation during both monotonic and cyclic loading (Agnew and Duygulu, 2005; Ando et al., 2010; Beyerlein et al., 2010). It has been further shown that grain-scale strain incompatibilities and texture effects in Mg-based alloys cause distinct and twin-related strain localizations (Barnett et al., 2012; Hazeli et al., 2013a,b, 2014). Therefore, localized strains near grain boundaries or second phase particles could cause, very high local stresses (Hull, 1999) that could lead to crack initiation. This article, therefore, focuses on the role of twinning–detwinning on fatigue damage initiation of Mg alloys. It further examines the effect of local microstructure on both the macroscopic mechanical response during strain-controlled fatigue conditions, as well as on local microstructural changes which are reported herein as key factors to characterize the fatigue behavior of Mg alloys. To accomplish these goals, an experimental approach consisting of mechanical testing of standardized-size specimens, *in situ* nondestructive monitoring and *ex situ* high resolution microstructural characterization tools was combined with an appropriately defined model, capable of incorporating dominant microstructural observations in its derivation.

## 2. Experimental procedure and modeling approach

### 2.1. Specimen preparation

A commercial magnesium alloy (AZ31) with a nominal composition of 3 wt.% Al and 1 wt.% Zn was used. The alloy was obtained as a 25.4 mm thick plate (see Fig. 1a) in the soft annealed condition (O temper). Before cutting any specimens, the material was held at 500 °C for one hour. Texture and the average grain size distribution, were measured in metallographic samples cut from the Normal Direction (ND) of the plate. The initial microstructure and measured texture are presented in Fig. 1b and c, respectively. Compression, tension, and fatigue specimens were machined from the Mg plate using Electrical Discharged Machining (EDM) according to ASTM E9, E8M, and E606 standards. Tension and fatigue tests were performed for samples cut parallel to the Transverse Direction (TD) direction, while compression tests were conducted for specimens cut from the different orientations shown in Fig. 1.

### 2.2. Mechanical and nondestructive testing

Monotonic compression and tension tests were performed at room temperature using a MTS universal testing system at a constant strain rate of  $4.5 \times 10^{-4} \text{ s}^{-1}$ . The same testing system was also used to apply strain-controlled, cyclic, compression–tension loading profiles for several values of peak strain. The fatigue tests were carried out at zero mean strain ( $R_\epsilon = -1$ , i.e. completely reversed sawtooth type strain cycle), at a constant rate of  $5 \times 10^{-3} \text{ s}^{-1}$ . Peak strain amplitudes equal to 0.25%, 0.33%, 0.42%, 0.50%, and 0.58% were applied. Furthermore, *in situ* nondestructive monitoring of the fatigue experiments was provided by application of the Acoustic Emission (AE) method. Signals (voltage versus time waveforms) of AE were recorded using a piezoelectric transducer (PICO manufactured by MISTRAS Group, Princeton, New Jersey) which has an operating frequency in the 200–750 kHz range and a peak frequency at 500 kHz. The AE sensor was connected to a 4-channel data acquisition board (DISP-4, MISTRAS).

### 2.3. Characterization methods

Fracture surfaces from the fatigued specimens were examined using Scanning Electron Microscopy (SEM). To study *ex situ* the effect of cyclic strain at the grain scale, fatigue tests were performed on specimens that were polished from one side to a finish sufficient for Electron Back Scatter Diffraction (EBSD) measurements. For this purpose, three regions of interest ( $500 \times 500 \mu\text{m}^2$  each) were marked by using micro-hardness indentation. Local grain information, including lattice orientations were measured at intervals of 1  $\mu\text{m}$  on a hexagonal grid by automated acquisition and processing of backscatter diffraction patterns in a SEM (FEI XL30). The accelerating voltage and working distance were set at 20 kV and 19.5 mm, respectively. The surface morphology in the marked region was inspected post mortem by non-contact white light interferometry using a

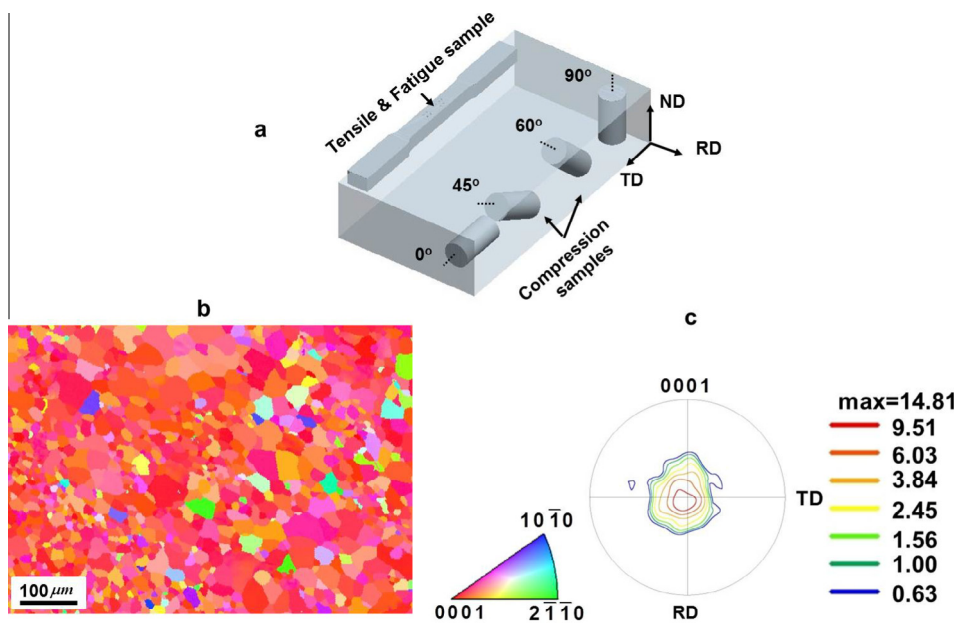


**Fig. 1.** (a) Compression, tension and fatigue sample preparation based on the as-received rolled plate. (b) Initial inverse pole figure map and (c) its corresponding pole figure.

Zygo surface profilometer (model 6300, Zygo Corporation, Middlefield, Connecticut) at 20× magnification. As a result of using an objective lens (20×, Mirau), lateral and vertical resolutions of 750 nm and 0.1 nm were achieved.

## 2.4. Modeling approach

To quantify the effect of activation of the available deformation mechanisms including twinning on the hysteretic fatigue behavior of the first two cycles a modeling approach based on the viscoplastic self-consistent (VPSC) scheme developed by [Lebensohn and Tomé \(1993\)](#) was used. Specifically, a Continuum Dislocation Dynamics (CDD) approach was developed in which slip, twinning and detwinning systems are defined by their corresponding normal and Burgers vectors, as well as their associated dislocation densities ([Li et al., 2013](#)). Recently, computational models for studying the detwinning mechanism based on twin nucleation and propagation ([Wang et al., 2012](#)), in addition to microstructure evolution during twinning ([Proust et al., 2009](#)) were proposed. In the present study, a model based on a phenomenological power law shear rate formulation that describes both twinning and detwinning as polar mechanisms was used. Specifically, it was assumed that twinning requires positive and detwinning requires negative resolved shear stress (RSS) with respect to the twinning Burgers vector. In addition, activation of detwinning in the model was only possible in the case of positive twin volume fraction. This is a physical requirement since detwinning is the inverse mechanism of twinning and it cannot be activated if a twinned region does not exist. Therefore the model allows the twinned volume fraction to recover and add to the untwinned volume fraction of the crystal by means of detwinning. Since this formulation only determines the plastic part of the deformation, the elastic strains are calculated separately. Specifically, assuming a homogeneous distribution of elastic strains for all grains, the obtained stresses from the model and the calculated elastic modulus of the polycrystal are used to determine elastic strains at each step. The plastic strain rate in each grain at a given time step is determined according to the shear rates in the slip and the twinning/detwinning systems. Furthermore, the strain rates and stresses in each crystal must conform self-consistently to the corresponding quantities in the homogenized polycrystal which is defined by the boundary conditions. Considering only the plastic part of deformation, the strain rate in each grain in the deviatoric space is represented by summation of shear rates in each deformation system as  $\dot{\epsilon}_{ij} = m_{ij}^s \dot{\gamma}^s$  where  $m_{ij}^s = (n_i b_j + n_j b_i)/2$  is the Schmid factor for slip or twinning system  $s$ , the normal vector to the deformation system is  $n$  and  $b$  is the Burgers vector. Given the deviatoric stress  $\sigma'_{ij}$ , the shear rate in each deformation system is assumed to be given as

$$\dot{\gamma}^s = \dot{\gamma}_0 \left| \frac{\tau^s}{\tau_{th}^s} \right|^{\frac{1}{m}} \text{sign}(\tau^s) \quad (1)$$

where  $\tau^s = m_{kl}^s \sigma'_{kl}$  is the resolved shear stress,  $m$  represents the strain rate sensitivity,  $\tau_{th}^s$  is the threshold stress to initiate deformation in a system  $s$  and  $\dot{\gamma}_0$  is a reference shear rate.

The strain rate equation defined previously contains five equations and ten unknowns. Therefore additional relationships for solving the system are required. The strain rates and stresses in each crystal must conform self-consistently to the strain rate and stress in the homogeneous media. Therefore, following a linearization of these quantities and by using the equivalent inclusion method ([Eshelby, 1957](#)) a linearized interaction equation between the quantities in the crystal and their pairs in the homogeneous media (shown in capitals) can be obtained using a grain interaction matrix  $M_{ijkl}$  and eigenstrains  $\dot{\epsilon}_{ij}^*$ .

$$\begin{cases} \dot{\epsilon}_{ij} = \dot{\gamma}_0 \sum_1^s m_{ij}^s \left( \frac{m_{kl}^s \sigma'_{kl}}{\tau_{th}^s} \right)^{\frac{1}{m}} \\ (\dot{\epsilon}_{ij} - \dot{E}_{ij}) - \dot{\epsilon}_{ij}^* = M_{ijkl} (\sigma'_{ijkl} - \Sigma'_{ijkl}) \end{cases} \quad (2)$$

Eq. (2) contains a set of ten equations and ten unknowns that can be solved following an iterative process. Different linearization techniques have been developed for Mg alloys and each one leads to a different self-consistent scheme ([Wang et al., 2010a, 2010b](#)). Among the different schemes, the Affine self-consistent scheme demonstrates the best overall performance and is therefore used in our modeling approach.

In the CDD model used instead of using the phenomenological model defined in Eq. (1) for describing the shear rate on each deformation system, Orowan's relationship for the shear rate in a slip system was used

$$\dot{\gamma}^s = \rho^s v^s b^s \quad (3)$$

where  $\rho^s$ ,  $v^s$  represent mobile dislocation density and their velocity as a function of stress respectively, and  $b^s$  is the corresponding Burgers vector. These quantities are assumed to be constant throughout the grain at each time step. In Eq. (3),  $v^s$  for each slip system is computed as follows

$$v^s = v_0^s \left| \frac{\tau^s}{\tau_{th}^s} \right|^{\frac{1}{m}} \text{sign}(\tau^s) \quad (4)$$

In Eq. (4),  $\tau^s$  and  $\tau_{th}^s$  are RSS and threshold stress, respectively, and  $v_0^s$  is a referenced velocity. The shear rate due to twinning or detwinning is assumed to be governed by a power law of the form:

$$\dot{\gamma}^{tw} = \begin{cases} \dot{\gamma}_0 \left| \frac{\tau^{tw}}{\tau_{th}^{tw}} \right|^{\frac{1}{m}} & \tau^{tw} > 0 \quad (\text{Twinning activity}) \\ -\dot{\gamma}_0 \left| \frac{\tau^{tw}}{\tau_{th}^{tw}} \right|^{\frac{1}{m}} & \tau^{tw} < 0 \text{ and } f^{tw} > 0 \quad (\text{Detwinning activity}) \\ 0 & \text{Otherwise} \quad (\text{No twinning or detwinning}) \end{cases} \quad (5)$$

Following the conditions presented in Eq. (5), the rate of twinning or detwinning is similar to the rate of slip in terms of the equations that control these mechanisms. Twinning and detwinning are polar mechanisms and require positive RSS in their plane and with respect to the direction of the Burgers vector. Therefore, twinning can only occur if the resolved RSS is positive with respect to the Burgers vector and detwinning can only occur if twins are available in the system and RSS is negative with respect to Burgers vector of twinning so that the existing twins retreat. The negative sign for detwinning shear rate implies that detwinning acts as a recovery mechanism for previous plastic deformation due to twinning similar to the retreat of the partial dislocations creating the twins. Note that this definition of twinning and detwinning systems automatically prevents activation of both mechanisms simultaneously. The additional condition defined in Eq. (5) for the detwinning system ensures that detwinning is only allowed when a positive volume fraction of the twins is available in the corresponding system to be “consumed”.

Furthermore, we assume that plastic deformation is caused by the activation of basal  $\{0001\}\langle 11\bar{2}0\rangle$ , prismatic  $\{1100\}\langle 11\bar{2}0\rangle$ , and  $\langle c+a \rangle$  pyramidal  $\{1122\}\langle 11\bar{2}3\rangle$  slip, as well as  $\{10\bar{1}2\}\langle 10\bar{1}1 \rangle$  extension twinning. The threshold stress in Eq. (5) evolves according to the general Voce law (Voce, 1955), but the threshold stress in Eq. (1) is represented by

$$\tau_{th}^s = \tau_0^s + \tau_{HP}^s + \alpha\mu b\sqrt{\Omega^{sr}\rho^r} \quad (6)$$

for slip systems, where  $\tau_0^s$  is the initial critical resolved shear stress,  $\tau_{HP}^s$  is the Hall–Petch hardening parameter and the third term represents the forest dislocation hardening (Ohashi et al., 2007). The last term in Eq. (6) captures the latent-hardening and self-hardening as proposed by the Bailey–Hirsch model, with  $\alpha$  being a constant,  $\mu$  the shear modulus and  $\Omega^{sr}$  the dislocation interaction matrix that defines the latent hardening effect of system  $r$  on system  $s$ . In addition, the dislocation density  $\rho^r$  is the sum of mobile ( $\rho_m^r$ ) and immobile ( $\rho_i^r$ ) dislocations in a system  $r$  which evolves according to the following equations (Askari et al., 2014):

$$\dot{\rho}_m^s = \alpha_1\rho_m^s \frac{v^s}{\bar{l}} - 2\alpha_2 R_c (\rho_m^s)^2 v^s - \alpha_3 R_c \rho_m^s \rho_i^s v^s - \alpha_4 \rho_m^s \frac{v^s}{\bar{l}} + \alpha_5 \left| \frac{\tau^s}{\tau^*} \right|^r \rho_i^s \frac{v^s}{\bar{l}} \quad (7)$$

$$\dot{\rho}_i^s = \alpha_4 \rho_m^s \frac{v^s}{\bar{l}} - \alpha_3 R_c \rho_m^s \rho_i^s v^s - \alpha_5 \left| \frac{\tau^s}{\tau^*} \right|^r \rho_i^s \frac{v^s}{\bar{l}} \quad (8)$$

The constants  $\alpha_1$ – $\alpha_5$  control the dislocation generation rate, mutual annihilation of mobile dislocation, annihilation of mobile and immobile dislocations, dipole formation rate and the rate at which immobile dislocations break up from locks and become mobile. In addition,  $R_c$  is the critical distance for dislocation reaction and  $\tau^*$  is the critical stress for unpinning, which is in the order of threshold stress and dislocation mean free path  $\bar{l}$ .

Although dislocation hardening is defined through the interaction matrix  $\Omega^{sr}$ , any other hardening that arises from dislocation and twin interactions is accounted for by the dislocation mean free path. Here we assume that twins are impenetrable regions inside the grain. Therefore twinning in this formulation is expected to reduce the available space for dislocation glide by reducing the mean free path, similar to Kalidindi’s approach (Kalidindi, 1998), and is presented by the following equation:

$$\bar{l} = \sqrt{\frac{1-f_{tw}}{\rho_{total}}} \quad (9)$$

In Eq. (9)  $f_{tw}$  is volume fraction of twins and  $\rho_{total}$  is the total dislocation density in the grain. The twin volume fraction rate in each grain is calculated by  $\dot{f}_{tw} = \sum \dot{\gamma}^{tw}/S^{tw}$  which is the sum of shear rates in twin systems obtained by Eq. (5) divided by the characteristic shear of the twin  $S^{tw}$  (Tome et al., 1991). In the case of detwinning activity, the volume fraction of the twins will be reduced and subsequently, softening in dislocation glide is expected. The complete specification of the parameters and dislocation evolution laws are presented elsewhere (Askari et al., 2014).

In Mg, the reorientation due to twinning is an important issue that needs to be considered in the modeling scheme. We use the predominant twin reorientation (PTR) scheme (Tomé et al., 1991) to capture this effect. The PTR scheme assumes that a grain is allowed to reorient rapidly if a specific accumulated value of twin fractions reaches a threshold value. Since it is not numerically feasible to consider each twinned fraction as a new orientation, the PTR scheme adopts a statistical approach. Since the twin volume fraction rate  $\dot{f}_{tw}$  is obtained by calculations, the volume fraction of twins is known at every step of calculations. After completion of each step, a grain is selected randomly and the most active twin system is identified. If the accumulated volume fraction of the twins for a system is larger than the threshold value, then the grain is allowed to reorient and the volume fractions and the threshold value are updated. The process is repeated until either all grains are checked or volume fraction of reoriented grains exceeds the accumulated volume fraction of the twins. Note that this process

leads to reorientation of the grains consistent to the historically active twin systems. Further details can be found in the literature (Tomé et al., 1991).

### 3. Results and discussion

#### 3.1. Monotonic behavior

Representative compression and tension stress–strain curves are plotted in Fig. 2. Compression normal to the rolling direction (RD) gave the highest yield stress, while remarkable elongation (>20%) can be obtained for the specimens cut at 45° with respect to the rolling direction. It should be noted that the yield stress decreases substantially when the specimen approaches the TD orientation (see Fig. 1a). Since the average grain size of the specimens was very similar, this observation can be attributed to the significant effect of texture on mechanical response. In fact, the high Schmid factor (SF) for twinning in TD compression (Wang and Huang, 2007) has been shown to result in the characteristic s-type stress–strain behavior (Barnett, 2007; Hazeli et al., 2013a; Kleiner and Uggowitzer, 2004). The mechanical behavior results in Fig. 2 show hardening differences between tension and compression (referred to as tension–compression asymmetry). In an extruded Mg alloy with strong basal texture it is expected that this asymmetry is largely determined by the relative ease with which tension twinning occurs (which dominates yielding in compression) compared to that of prismatic slip (which dominates yielding in tension, (Robson et al., 2011)).

#### 3.2. Cyclic behavior

The fatigue deformation behavior during the first and second cycle, as well as half-life and at one cycle before failure are shown in Fig. 3. As the initial texture is favorable for twinning in the compressive loading path, there is a plateau in the stress–strain curve past the corresponding yielding point in agreement with pertinent fatigue results (Wu et al., 2008a, 2010, 2008c). The region of constant stress, as mentioned previously, corresponds to twinning (Barnett et al., 2012; Hazeli et al., 2013a). Significant tension–compression asymmetry can be observed upon load reversal (Barnett, 2007; Wu et al., 2008a), which becomes more pronounced with increasing strain amplitude. This increase can be justified by the fact that the twin density is expected to increase by increasing strain amplitudes. While the reason for the observed Bauschinger-like effect has been proposed to be a result of the twinning–detwinning activity (Jordon et al., 2011; Park et al., 2010a), no validated explanation for its evolution and saturation has been given. Twinned regions formed in the compressive loading path reorient under subsequent tensile loading in which detwinning occurs (Hyuk Park et al., 2010), a process that is also possible to lead to plastic strain recovery. The compression–tension asymmetry reduces as the number of cycles increases. However, even near the end of the fatigue life, and especially at higher strain amplitudes, the hysteresis loop develops a noticeable inflection point as the load reverses from compressive to tensile. This could be attributed to detwinning even at the very end of the fatigue life, which is investigated further in this article. These inflection points are additionally indicative of macroscopic strain hardening that has been frequently attributed to dislocation interactions.

In agreement with the relevant literature (Begum et al., 2009; Hyuk Park et al., 2010; Matsuzuki and Horibe, 2009), the current results indicate strong variations in fatigue behavior, especially at higher imposed strain amplitudes. To quantify such variations the measured fatigue loops were characterized in terms of parameters shown in Fig. 4. This diagram defines the

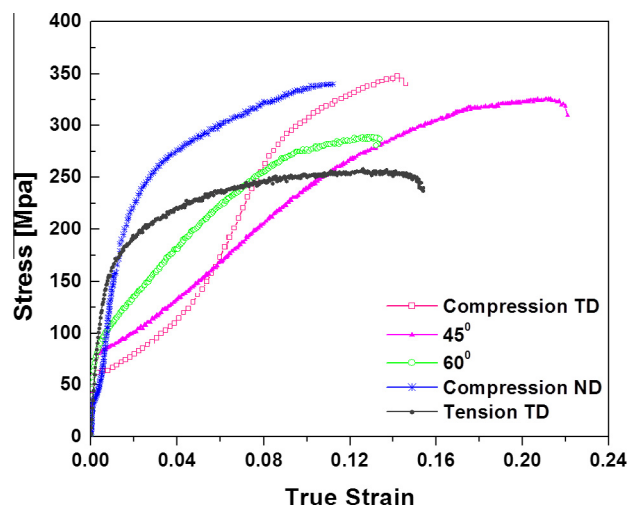


Fig. 2. Measured stress–strain curves for several specimens both tensile and compressive.

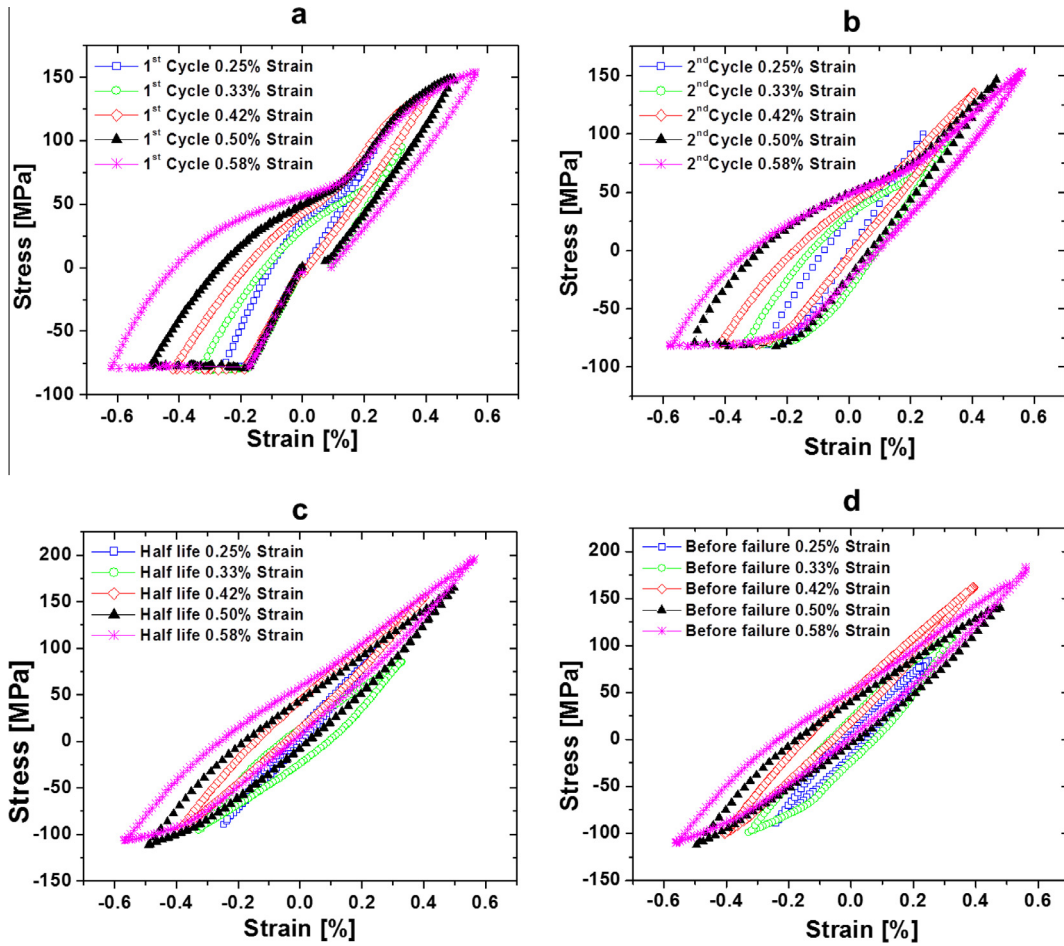


Fig. 3. Asymmetric hysteresis loops for varying applied strain amplitudes of 0.25, 0.33, 0.42, 0.5 and 0.58 under fatigue loading parallel to the transverse direction for (a) 1st cycle, (b) 2nd cycle, (c) half-life and (d) last loop before final failure.

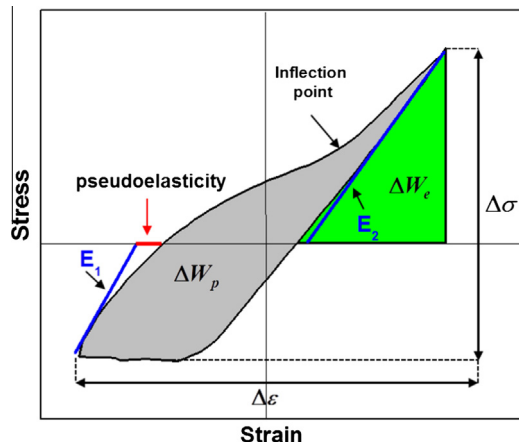


Fig. 4. Definition of hysteresis loop parameters.

compressive and tensile stiffness values  $E_1$  and  $E_2$ , the measured stress amplitude  $\Delta\sigma$ , the plastic strain energy density  $\Delta W_p$  and pseudoelasticity upon load reversal. It also shows characteristic inflection point in the tensile loading path. To determine the inflection point, the numerical derivative of the fatigue hysteresis curve was calculated and the inflection point was consequently approximated by identifying the transition point from low to high values (valley point) of the derivative.

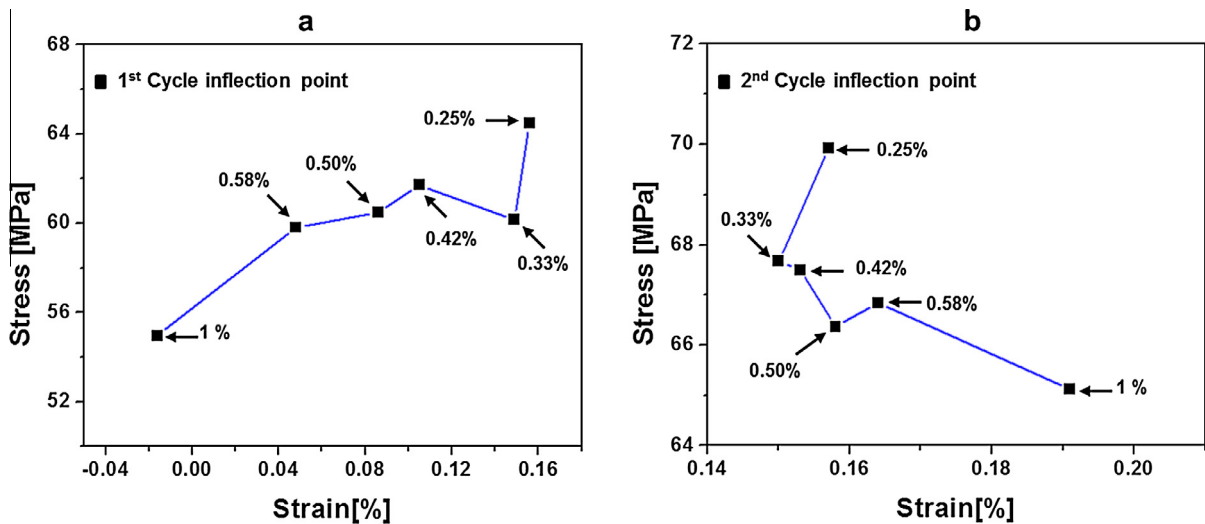


Fig. 5. Inflection points measured for (a) 1st and (b) 2nd fatigue loop at different imposed strain amplitudes indicated as percentage values for each inflection point.

The inflection point in Fig. 4 is used to describe the point where the strain hardening rate changes from descending to ascending. Fig. 5 presents the stress and corresponding strain for such inflection points for different strain amplitudes in the 1st and 2nd fatigue cycles. During the 1st cycle, the inflection points shift to higher levels of strain and stress as the imposed strain amplitude decrease. To explain this result, it should be kept in mind that strain hardening is very sensitive to the imposed strain amplitude, and that the increase in hardening rate correlates with exhaustion of twinning–detwinning (Wu et al., 2008a). In fact, the activation of harder slip systems, such as prismatic, is needed to accommodate further imposed strain when twinning–detwinning activity cannot accommodate any *c*-axis strains. This could explain the considerable change in strain hardening during tensile loading in the 1st fatigue cycle (Park et al., 2010b). During the second tensile loading cycle, similar inflection points are found at comparatively larger strains and stresses for each imposed fatigue strain amplitude (Fig. 5b). The difference in the corresponding stress for each inflection point between the first and second cycle was found to be more significant for the larger values of the imposed strain amplitude. This observation could be explained by the fact that by imposing larger fatigue strains potentially larger twin volume fractions are also created. Consequently, a larger volume fraction of twins is available to be detwin and thereby more tensile strain can be accommodated by detwinning. This is in accordance with *in situ* neutron diffraction results carried out by Wu et al. (2008a).

(Fig. 6) illustrates the evolution of compressive ( $E_1$ ) and tensile ( $E_2$ ) stiffness values as a function of the number of fatigue cycles. Both stiffness parameters were found to have their highest values at the smallest applied strain amplitudes. For  $E_1$  a sudden drop is observed after the first few loading cycles that are followed by an almost steady state response, whereas a more gradual change is seen for  $E_2$ . Similar observations were reported by Begum et al. (2009). Such changes in stiffness have been suggested to be the consequence of opening and closing of microcracks (Eisenmeier et al., 2001; Yin et al., 2008b). It can be also seen in Fig. 6 that the curves for the evolution of both stiffness parameters change rates with increasing fatigue cycles which is further explored in association with microstructural changes as described later in this article.

Fig. 7 shows the effect of different strain amplitudes on the maximum, minimum, and mean stresses as a function of fatigue life. The results presented in Fig. 7a demonstrate that the maximum stress increases, as expected, as the imposed fatigue strain amplitude increases. It is interesting to note that for the lower strain amplitudes (0.25% and 0.33%) the measured maximum stress has a slight decreasing trend during fatigue, whereas the higher imposed strain amplitudes lead to an increasing trend of the maximum stress per cycle as fatigue progresses. Furthermore, Fig. 7a demonstrates that the minimum stress per cycle decreases with evolving fatigue. This remark, in combination with the observed hysteresis loop shape changes past the 1st fatigue cycle, indicates that microstructural changes including changes in the twinning and slip activity cause changes in the hardening behavior depending on the imposed fatigue strain amplitude.

Moreover, the mean level of the imposed strain is known to play an important role in fatigue life (Suresh, 1998). Fig. 7c shows that for higher strain amplitudes the mean stress values per cycle initially decrease and then increase. A similar initial reduction and subsequent increase in mean stress is also reported in prior studies (Begum et al., 2009; Hasegawa et al., 2007). It is noted that the observed drop could be indicative of microscale damage (Hasegawa et al., 2007), which is consistent with sudden stiffness changes discussed earlier. Fig. 7c also suggests that the higher the mean stress, the shorter the fatigue life. It is remarkable that the higher imposed strain amplitudes lead to increasing mean stress values which could be another implicit indication of a more pronounced strain hardening behavior, again due to more significant changes in the deformation mechanisms compared to the smaller strain amplitudes.

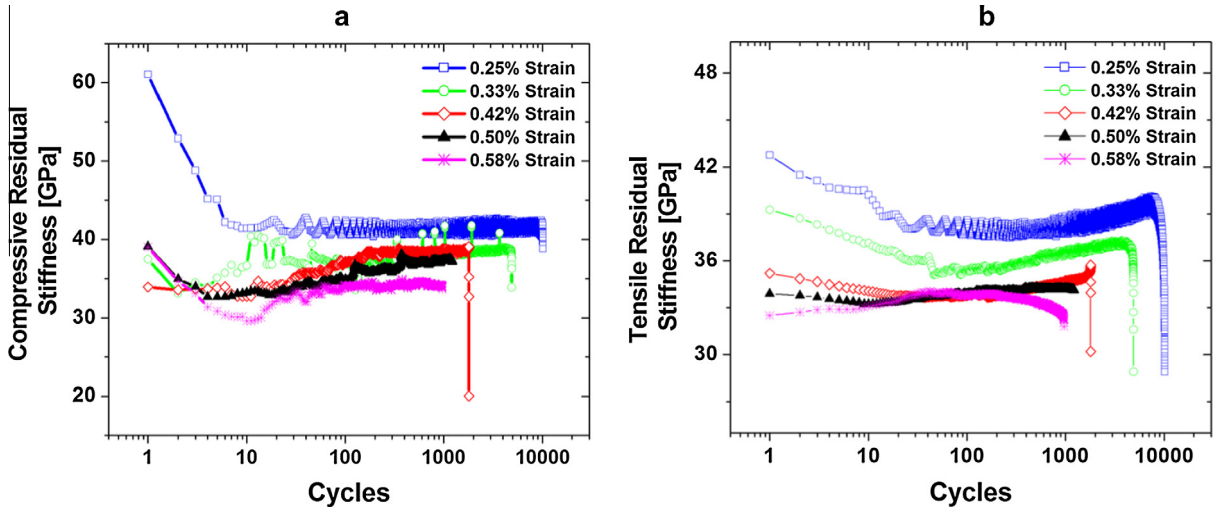


Fig. 6. Evolution of: (a) compressive and (b) tensile stiffness as a function of fatigue cycles.

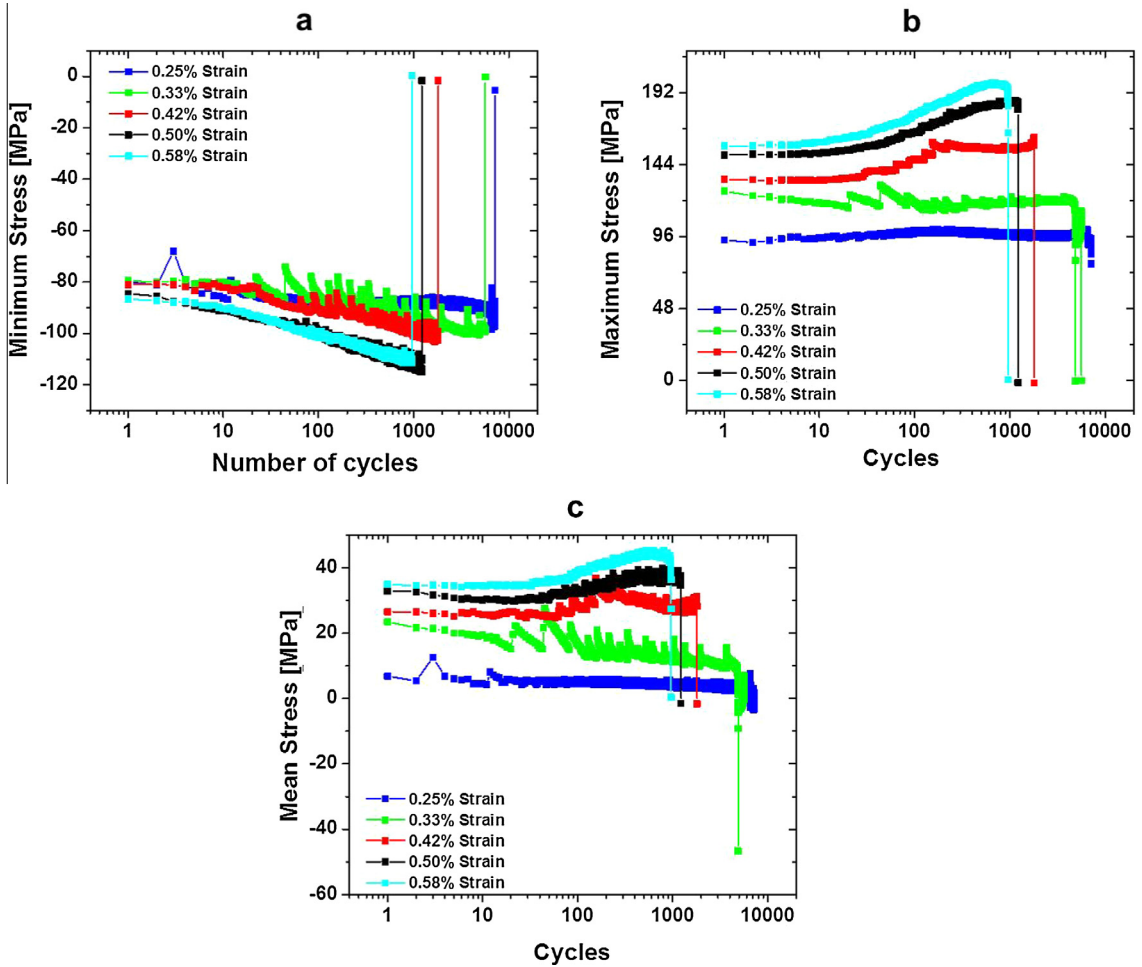


Fig. 7. Evolution of (a) maximum, (b) minimum and (c) mean stress for different imposed strain amplitudes.

### 3.3. Microstructure effects and fatigue crack initiation

Twinning–detwinning and partial twin removal have been reported in the literature (Caceres et al., 2003; Lou et al., 2007). Recently, Yin et al. (2008a) highlighted the key role of twinning–detwinning on microstructural evolution and cyclic hardening. However, direct evidence of this phenomenon and its association with fatigue in Mg alloys is scarce. Fig. 8 provides a microstructure-informed analysis of the macroscopic fatigue results discussed in the previous section for three different regions during compression and subsequent tension. Therefore, fatigue test was interrupted at 1% strain and the targeted spots were examined during compression and tension using EBSD. This approach allowed us to investigate the effect of loading path on the microstructure evolution. A closer look at this Figure reveals the occurrence of twinning–detwinning at the same region for three different locations as a direct result of a fatigue. Several twinning–detwinning occurrences in different grains during the same fatigue cycle in multiple regions in the material's microstructure are observed (Fig. 8b). The most important fact to note is that these measurements were performed using standard-sized specimens which incorporate the effect of the bulk, and consequently, are important from both a statistical and mechanical behavior points of view.

Real-time volumetric inspection of the fatigue behavior was conducted through the AE nondestructive method. In Fig. 9, the measured sawtooth stress–time curves for several fatigue cycles are overlaid with recorded AE signals for two different imposed strain amplitudes. These results show that the AE amplitude distribution (notice the top row of arrows) exhibits distinct increases near the peak compressive load, which agrees with previously reported results by the authors in monotonic tests (Hazeli et al., 2013a; Lu et al., 2008) which were directly related through microstructural analysis to the onset of twinning. The results in Fig. 9 suggest that the peak AE amplitude values recorded during compression (top set of arrows) are consistently much higher compared to the corresponding peak AE amplitude values (bottom set of arrows) recorded during tension. This observation could be attributed to the fact that the activation energy for twinning is larger than that for detwinning, presumably because of the need for nucleation, while it is further higher than the energy required to grow a twin. By comparing the decrease of the recorded AE amplitudes as a function of time, the hypothesis is made that the twinning–detwinning activity is possible to evolve as fatigue evolves. The difference though in AE amplitudes in compression and tension remains nearly constant (~25 dB difference) which might imply that initial twin nucleation as well as twinning–detwinning might operate for several cycles. As specified earlier, it is important to note that both stiffness and mean stress drop after the first loop, which could be an indication of either micro-cracking or twinning. However, twinning appears to be the most probable case for this effect based on the results in Fig. 8 (in which no microcracks were observed) and on the fact that the highest AE peak amplitude appears to occur repeatedly at the same loading value during compressive loading in the fatigue tests.

Twinning is recognized to be a major source of strain localization phenomena in Mg alloys (Hazeli et al., 2013a). In this framework, the authors recently used several experimental characterization techniques to show that twinning leads to

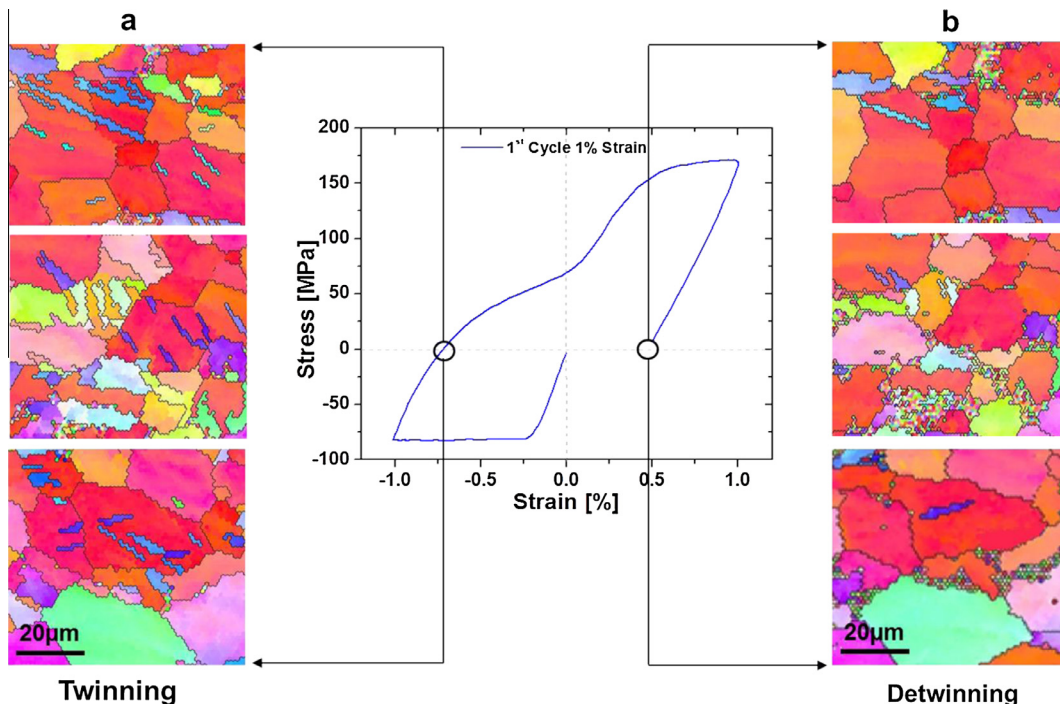


Fig. 8. First fatigue cycle for 1% imposed fatigue strain amplitude. (a) Twinning and (b) detwinning were identified for three different regions.

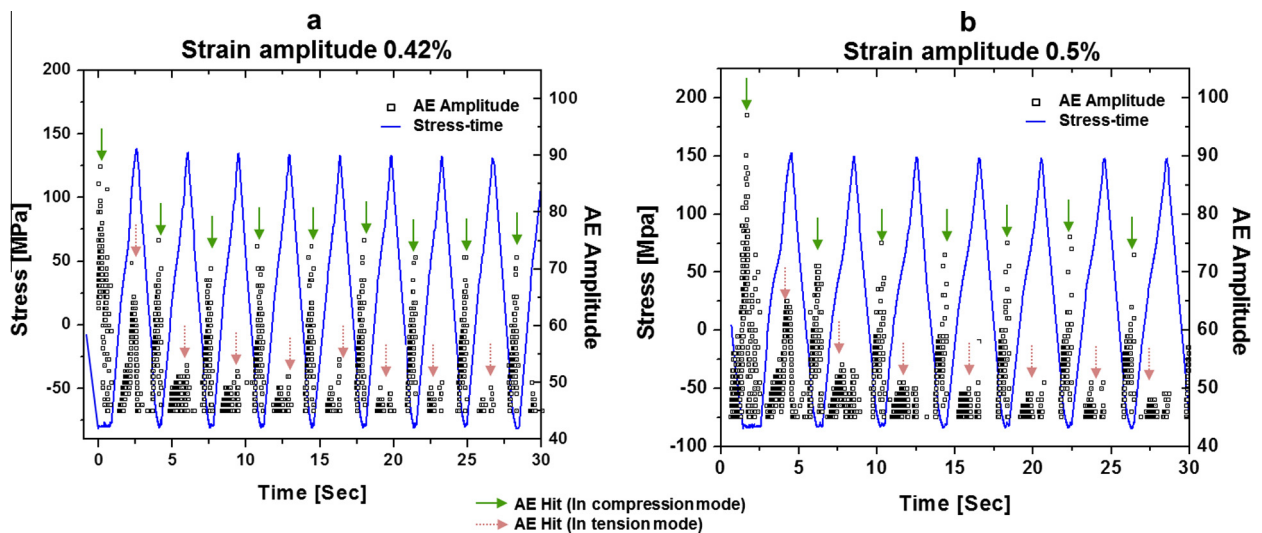


Fig. 9. Measured stress–time combined with real time AE activity: (a) strain amplitude of 0.42% (b) strain amplitude of 0.5%. Arrows indicates larger AE activity during compression than tension.

considerable surface extrusions and intrusions during monotonic loading (Hazeli et al., 2014). A similar approach was applied in this article to investigate the surface evolution of Mg alloys subjected to fatigue. To this aim, fatigue specimens prepared according to ASTM606-04 were polished to mirror surface finish. Several regions on the polished surface of each specimen were marked using a micro indenter to study surface parameters by using optical interferometry before and during fatigue. With the aid of these fiducial markers it was consequently feasible to inspect the same regions of interest at different stages of fatigue life. Fig. 10 shows relevant measurements in which the surface topography of a  $65 \times 85 \mu\text{m}^2$  region of the fatigued specimens at quarter-life, half-life and third-quarter life is presented. To quantify the observed surface topography, Fig. 10d shows the representative average of 3 scan lines across the longer side of the region in the direction of the points from i to ii. Note that for comparison purposes, care was given to terminate the fatigue loading always at the same point of stress ( $\sigma = -15 \text{ MPa}$ ). It is evident from the results in Fig. 10 that the surface morphology which was formed at quarter life is relaxed at fatigue half-life, while it becomes more pronounced at the third-quarter. This measurement provides indications of reversible surface roughening of Mg alloys during strain-control fatigue. This might also be a first indication of collective macroscopic effects of the twinning–detwinning process based on results previously reported (Hazeli et al., 2014) as it is further explored in this section.

It was specified earlier in this article that twinning could also be responsible for a non-zero mean stress during cyclic loading. In this regard, it was suggested that the twins and their parent grains must contain significant internal stresses that can start the detwinning immediately upon unloading (Wu et al., 2008b). Such large internal strain gradients as a direct result of twinning have been recently identified and quantified (Hazeli et al., 2014). It has been further suggested that the position of the twins in the deformed state is unstable, and that an opposing driving force could cause detwinning upon unloading (Caceres et al., 2003), which is also related to the pseudoelasticity observed during unloading following compression. In contrast, unloading from the peak tensile stress occurs elastically (Wu et al., 2008a).

In this context, further information on the twinning–detwinning activity during quarter, half and third quarter fatigue life is presented in Fig. 11. These results show EBSD measurements for the same region of the polycrystal at three different stages of the fatigue test. Similar to Fig. 8 a closer look at the twinning activity especially on the larger grain towards the top part of the microstructure indicates that not only a portion of the twin volume fraction can detwin as fatigue occurs but it is further possible to continue this apparently reversible twinning activity for up to the third quarter of the fatigue life. Based on this observation the hypothesis can be made that reversible twinning is possible to operate for the longer part of the fatigue life. This behavior is called twinning–detwinning–retwinning (TDR) in this article, to indicate that twinning does not saturate during early stages of fatigue, as it was previously reported (Geng et al., 2013; Hasegawa et al., 2007; Matsuzuki and Horibe, 2009) but it could remain active at least for sufficiently high imposed strain amplitude values. This observation along with the recorded AE amplitude (Fig. 9) suggests that the continuous evolution of mean stress (Fig. 7c) as noted by Park et al. (2010a) is governed by slip along with slip–slip, slip–twin, slip–twin impingements, texture hardening and probable local softening due to twin reversibility (Jiang et al., 2007; Koike, 2005). Although, neither the nondestructive nor the direct microstructural evidence provided in this article could quantify the relative contribution of the aforementioned evolutionary microstructural changes, the results in this article provide experimental evidence that these complex microstructural interactions, including a prolonged twinning activity appear to dominate the fatigue behavior of Mg alloys.

The effect of slip, twinning and TDR on crack initiation is discussed next. Fig. 12 presents an analysis of the possible crack initiation process of Mg alloys at the grain scale. It can be seen in Fig. 12a that for the targeted grain two distinct tensile twins

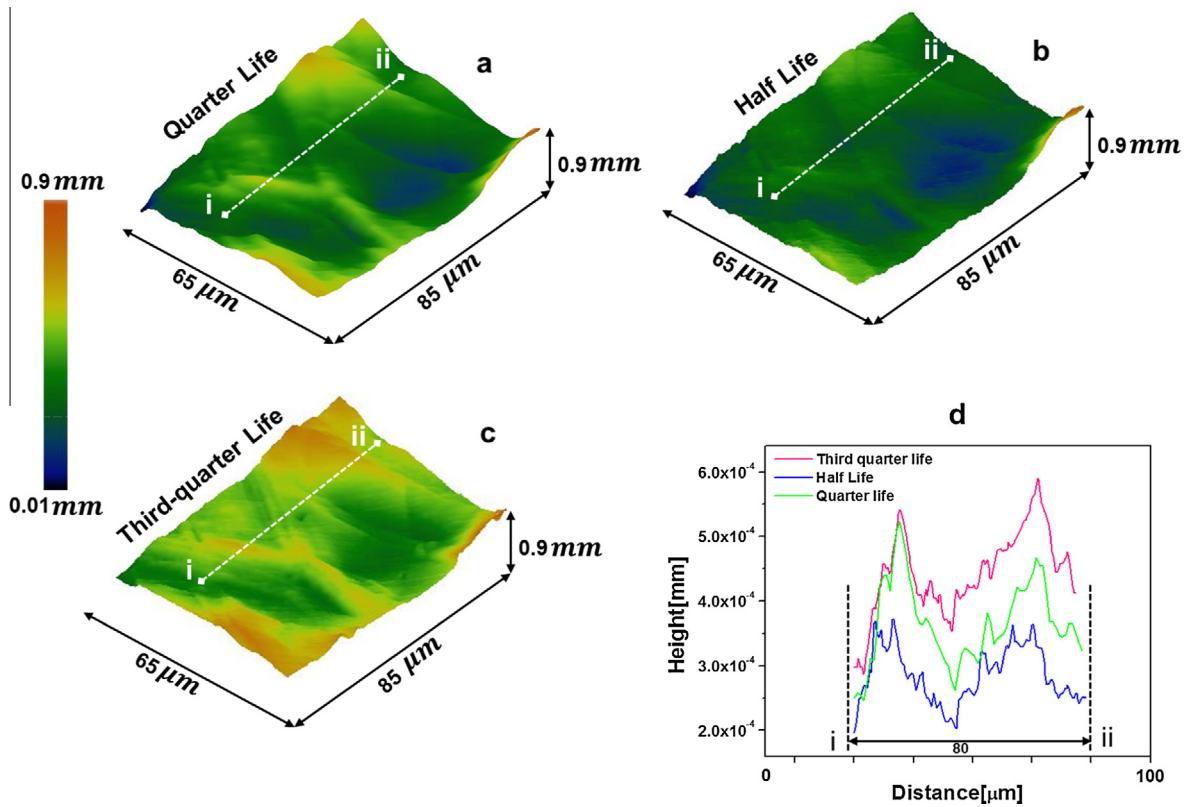


**Fig. 10.** Surface morphology of fatigued samples using strain amplitude of 0.5%, after fatigue (a) at quarter life, (b) half-life and (c) third-quarter life. The data were taken from samples which were polished to a mirror finish prior to cyclic loading. (d) Surface line scan starts from point i to ii. The surface trace lines were obtained from the average of three exact lines in the same neighborhood.

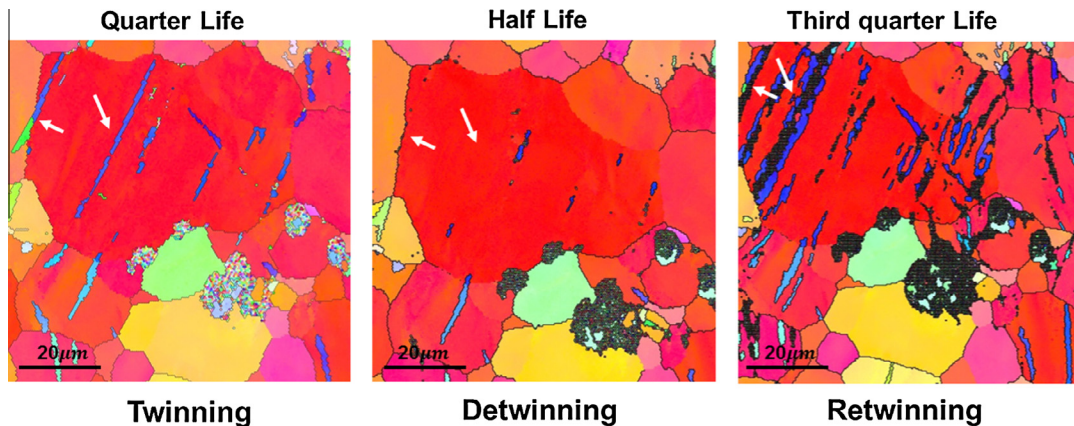


**Fig. 11.** Direct evidence of the Twinning–Detwinning–Retwinning (TDR) activity throughout the fatigue life. The EBSD maps were measured at 2000 $\times$  with step in the same region.

were formed (the nature of the twin was examined by misorientation analysis using EBSD software). In the case of the central twin, due to large surface distortions (Hazeli et al., 2014), only five points along the twin region were detected. However, they were sufficient to verify the characteristic  $\sim 86^\circ$  misorientation with respect to the original grain. This measurement was also super imposed on the EBSD pattern quality in Fig. 12b, which is dependent on sample topography (Trager-Cowan et al., 2007). The highly distorted region between two twins (quantified in Fig. 12d–f) could result from the high activation of slip systems as denoted by the dotted circles in Fig. 12b. Moreover, Fig. 12c represents a high quality SEM image of the same grain. It should be noted here that aside from the evidence provided by Yang et al. (2008) and despite

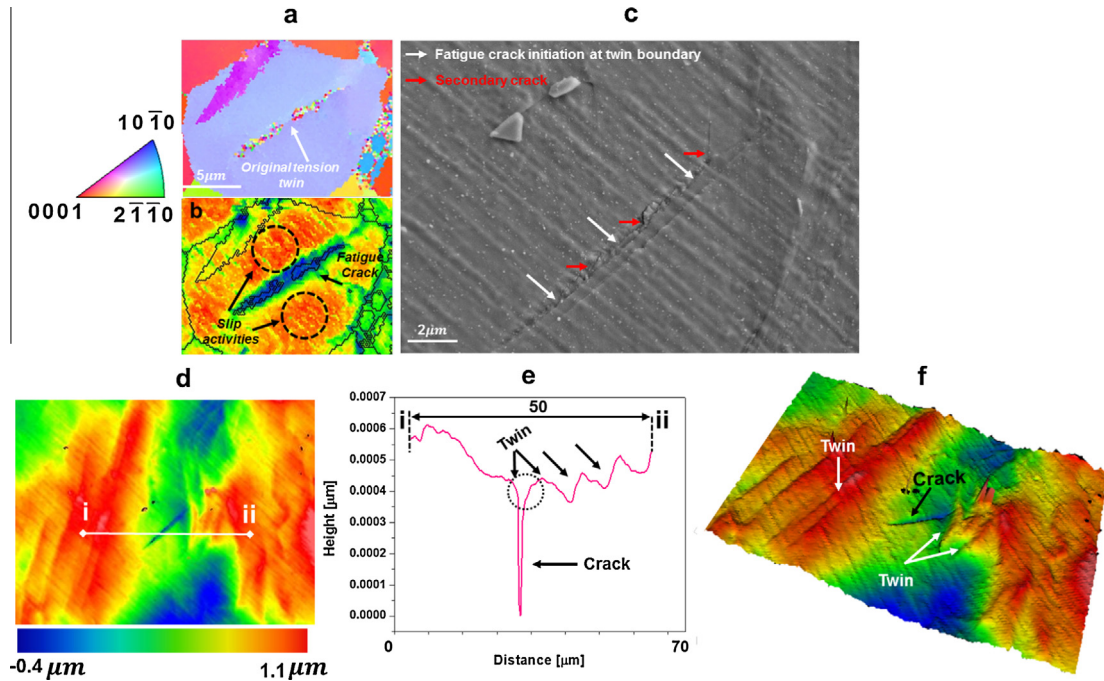


**Fig. 12.** (a) Super-imposed inverse pole figure on grain structure, from the sample fatigued up to its third-quarter of total life. (b) EBSD pattern quality demonstrating surface distortions due to operating deformation mechanisms at the grain scale. (c) High quality SEM image showing crack initiation along the twin boundary. This image also shows submicron cracks that form from larger crack along the twin boundary. (d) Surface morphology contour map. (e) Surface step profile from a line scan (average of three similar scans) along points i and ii. (f) Surface contour in 3D space displaying grain scale extrusions and intrusions due to twinning and fatigue crack formation.

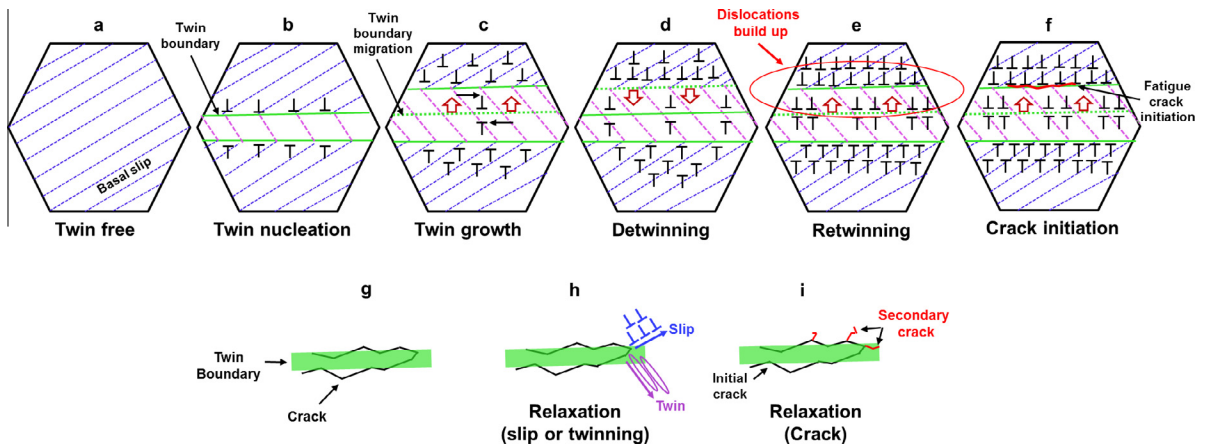


**Fig. 13.** Schematic illustration of a possible grain scale process involving slip and twinning that ultimately leads to formation of fatigue loading induced micro-cracks: (a) Basal slip lines in a grain. (b) Twinning occurring to accommodate strain along the *c*-axis. (c) Twin growth as a function of macroscopically imposed strain. (d) Twin nucleation and growth can be partially/fully reversed by accumulation of strain inside the twin or by application of reversed macroscopic loading. (e) Exhaustion of twinning–detwinning leading to localized strain accumulations. (f) Twinning–detwinning–retwinning occurs continuously and ultimately leads to micro-crack formation. Once a crack formed (g) the stress field around it can be relaxed by activation of additional slip/twin or (h) secondary cracking.

the great interest in identifying crack formation during fatigue of Mg alloys, no other experimental data was found in the relevant literature. In agreement with Yang et al., Fig 12c clearly shows that fatigue microcracks originate at twin boundaries. A closer view of Fig. 12c shows submicron crack formations at the side of the larger crack, in addition to the large crack along the twin boundary. In this context, Koike (2005), followed by Ando et al. (2010) found that in polycrystalline Mg, twinning occurs in a grain in which basal dislocations reduce large strains caused by large deformation gradients, e.g. such as the ones that could be created by the surface morphology quantified in Fig. 12d–f. It was also recently observed that the crystal

reorientation as a result of twinning leads to considerable surface steps, which produce a concentrated strain field within the grain (Hazeli et al., 2014). Thus, in order to satisfy the strain compatibility between the slip bands and twin, Yoo (1981) and Ando et al. (2010) suggested the formation of another slip, crack or secondary twin. The results in Fig. 12e and f demonstrate the existence of several 3D steps exactly at twin locations, as well as the formation of a crack in the region between the two twins. Therefore, it can be suggested that the combined effect of twinning, surface morphology, slip and their localized interactions create appropriate conditions for fatigue crack initiation at the subgrain level.

(Fig. 13) schematically visualizes the sequence of events suggested by the authors that lead to fatigue damage initiation in Mg alloys. As noted earlier, for the favorably oriented grains, twinning usually occurs in a grain in which slip operates abundantly (Fig. 13a). Twin formation may occur as a consequence of a mechanism operated to reduce the strain caused by slip (Fig. 13b). Subsequent loading leads to twin boundary disassociation (twin growth in Fig. 13c) as function of imposed strain, which can be reversed as the loading direction changes (detwinning in Fig. 13d). Additional load reversals could lead to the formation of new twins (retwinning in Fig. 13e) which was the reason this process is referred to as TDR in this article. TDR is suggested to occur for a large portion of the fatigue life. The repeatable operation of twinning–detwinning leads to plastic localization within the grain, which could be the result of dislocation accumulation also produced to relax the pronounced surface steps reported in this article and previously by the authors (Hazeli et al., 2014). Therefore, it is highly probable that the fatigue crack initiates at twin boundaries as shown in Fig. 13f. This assumption is based on the experimental observation given in Fig. 12c. As further depicted in Fig. 13g–i, the fresh crack could be relaxed with either additional slip or twinning. Secondary cracks can also form (Fig. 13i) to reduce local strain incompatibilities.

### 3.4. Fractography

Fig. 14 shows SEM fractography information revealing microcrack formation at regions near the surface. To quantify features within this fracture surface, three regions were used in Fig. 14b while higher magnification details are presented in Fig. 14c. These regions correspond to nucleation, initiation and are followed by what is termed as rapid fracture zone. Higher magnification images in Fig. 14c show the formation of microcracks near twin lamina that could be dominant fracture

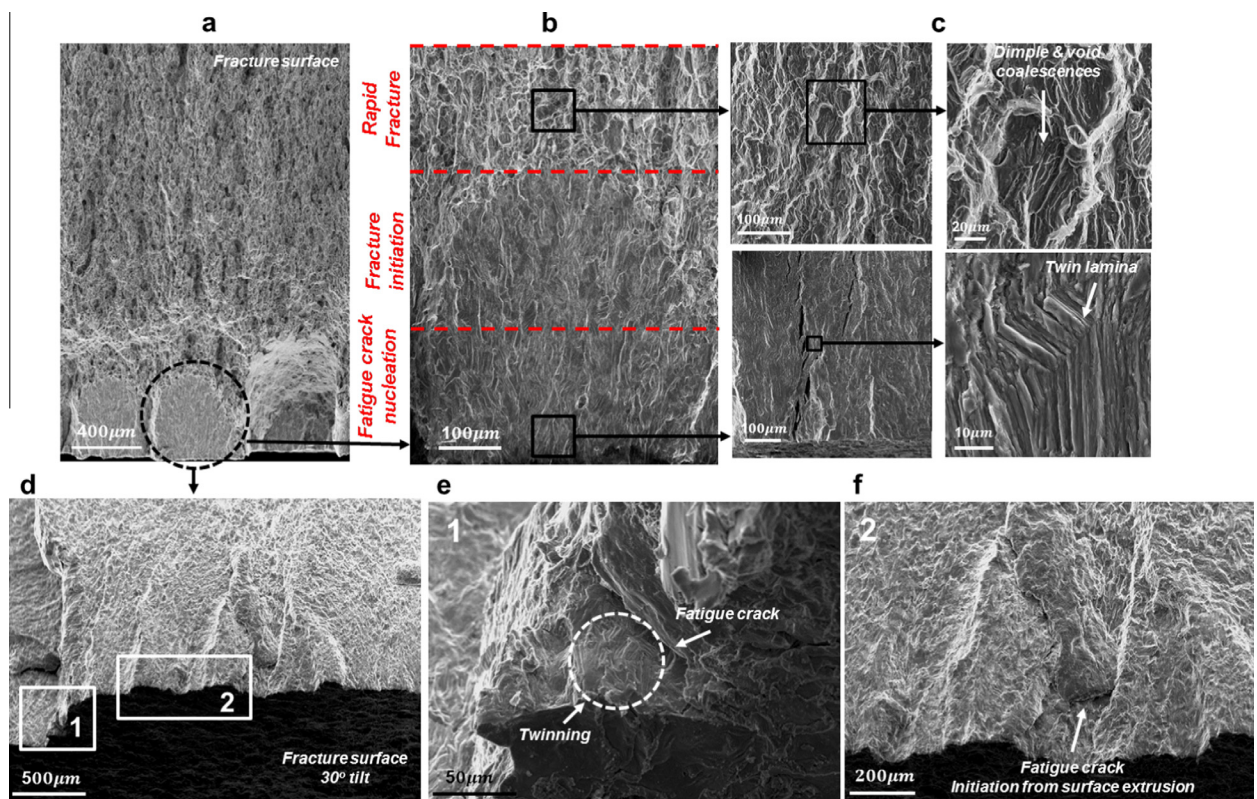


**Fig. 14.** (a) Fracture surface topography of the fatigue specimen tested with 0.5% amplitude and (b) stages of fatigue damage occurrence labeled as nucleation, initiation and rapid fracture. (c) High magnification SEM images from the crack region showing the existence of lamellar structure due to twinning. Corresponding high magnification SEM observations from the center of the specimen displaying a dimple-like topography. (d) Tilted view of the fracture surface which allowed the observation of 3D features such as surface steps labeled in two numbered areas. (e) High magnification images showing cleavage surface formation across pre-existing twin, and (f) fatigue crack formation along a surface extrusion.

nucleation sites. In comparison, more ductile type fracture patterns are observed in the rapid fracture zone, which is characterized by dimple formation as a result of e.g. void coalescences. A tilted view is used in Fig. 14d–f to further quantify features of the fractured surface. A noticeable cleavage type fracture at the surface (area numbered as “1”) and a dimple pattern at the center of the SEM image (area marked as “2”) are shown in Fig. 14d. Higher magnification images of these two areas reveal a large number of twins having lamellar structure (Fig. 14e), while it was also found that the fatigue cracks are bordered by twins at surface extrusion locations (Fig. 14f) in agreement with previous results in this article. Based on this information it is possible to assume that when a crack crosses a twin the microstructure tilts locally, leading to this cleavage topography. This could further indicate that in the presence of twinning, or due to their formation during fatigue, the crack front separates in the plane between the twin and original microstructure (Brooks and Choudhury, 2002; Hull, 1999). The observed surface fatigue damage appears, therefore, to be composed of twin-assisted cracks.

### 3.5. Crystal plasticity modeling

The experimental information provided in this article shows evidence on the significant role of twinning and detwinning on plasticity and damage initiation of Mg alloys. The modeling framework described in Section 2.4 was used and compared with the experimental results presented in Section 3.2. Specifically, data obtained from EBSD measurements including 194 orientations were used to represent the polycrystal in the model. Table 1 presents major parameters used in this approach. These values were found according to the literature and by curve fitting to the monotonic stress–strain curves for strain amplitude of 0.5% shown in Fig. 2. The strain rate sensitivity  $m$  was set to be 0.05, the parameters  $\alpha_2 = 1$  and  $\alpha_3 = 0.02$  were used for all slip systems, while the critical distance  $R_c$  was set to  $25b$  where  $b$  is the Burgers vector magnitude (equal to  $2.54 \times 10^{-10}$  m for Mg). The threshold stress for twinning systems was set to 38 MPa; for detwinning systems the initial threshold was set to 10 MPa at early stages of detwinning, during which small twinned regions begin to detwin. This value was then rapidly increased to 38 MPa to reach the same threshold stress as the twinning systems. With regards to the applied boundary condition, it is shown in Section 3.3 that the transverse direction exhibits surface roughening which is an indication of un-deterministic strain rate in these two directions. Therefore, it was essential to define appropriate boundary conditions in the model to reduce deviations from experimental results. To this aim, a strain rate boundary condition in the loading direction was imposed to allow for disturbances of the strain rate in the transverse direction, while enforcing normal stresses to zero. These boundary conditions – in contrast to conventional ones employed in the relevant literature in which the strain rate in the transverse direction is set equal to the negative half of the strain rate in the loading direction – increased the capabilities of the modeling approach and further prevented induced stresses in the transverse direction.

Common practice in modeling cyclic behavior with the VPSC scheme is to start from a completely determined velocity gradient tensor as the boundary condition, i.e. to set the strain rate in the transverse direction equal to negative half of the applied strain rate. However, the current experimental results (Fig. 10) suggest that this boundary condition is not accurate due to appearance of surface ripples as a direct result of twinning and detwinning. Therefore, stress was used as the boundary condition in the transverse direction, while strain rate was computed as a function of load. Due to this assumption more variation was achieved in the strain rate, which is consistent to its physical nature. It is further shown in this section that this approach results in excellent agreement between modeling and experimental results for the first two cycles as the attempt here was to incorporate this significant experimental measurement into the crystal plasticity based model and track its effect on the changes in the hardening behavior and not to predict the fatigue life.

Fig. 15 compares simulation results with experimental data for different strain amplitudes under compression–tension loading conditions which shows good agreement. For all strain amplitudes, the compression curve starts as a plateau since plasticity is mostly dominated by twinning at these small strains (Barnett et al., 2012; Hazeli et al., 2013a; Muránsky et al., 2010). At this stage basal slip is also active but due to weak interactions of basal dislocations, only small changes in the hardening rate were computed. Upon load reversal and due to the activation of detwinning, much of the hardening in the compression stage is reversed because of the decrease of twin volume fraction. According to Eq. (9) this process increases the mean free path for dislocation motion and it can consequently cause easier dislocation glide. After detwinning saturates as a result of consumption of the twinned regions, the harder to activate prismatic and pyramidal systems accommodate additional deformation; because of their strong interactions (as defined in Table 1) rapid increase in the hardening rate is observed.

**Table 1**  
CDD-VPSC parameters for AZ31. Values of  $K$  are reported from Raeesinia et al. (2011).

Parameter	Basal	Prismatic	Pyramidal twin
$\tau_0$ (MPa)	5	55	65
$\alpha$	0.3	0.3	0.3
$\alpha_1$	0.2	0.05	0.05
$\alpha_4$	0.02	0.02	0.05
$\rho_m^0, \rho_i^0$ (m <sup>-2</sup> )	$4 \times 10^{11}$	$1.5 \times 10^{11}$	$0.6 \times 10^{11}$
$\Omega$	$\Omega^{\text{basal}} = 0.2, \Omega^{\text{Prismatic}} = 1.0, \Omega^{\text{Pyramidal}} = 1.5$	$\Omega^{\text{basal}} = 1.0, \Omega^{\text{Prismatic}} = 0.2, \Omega^{\text{Pyramidal}} = 1.5$	$\Omega^{\text{basal}} = 1.0, \Omega^{\text{Prismatic}} = 1.0, \Omega^{\text{Pyramidal}} = 1.0$
$K$ (MPa/mm <sup>2</sup> )	0.42	3.72	4.71

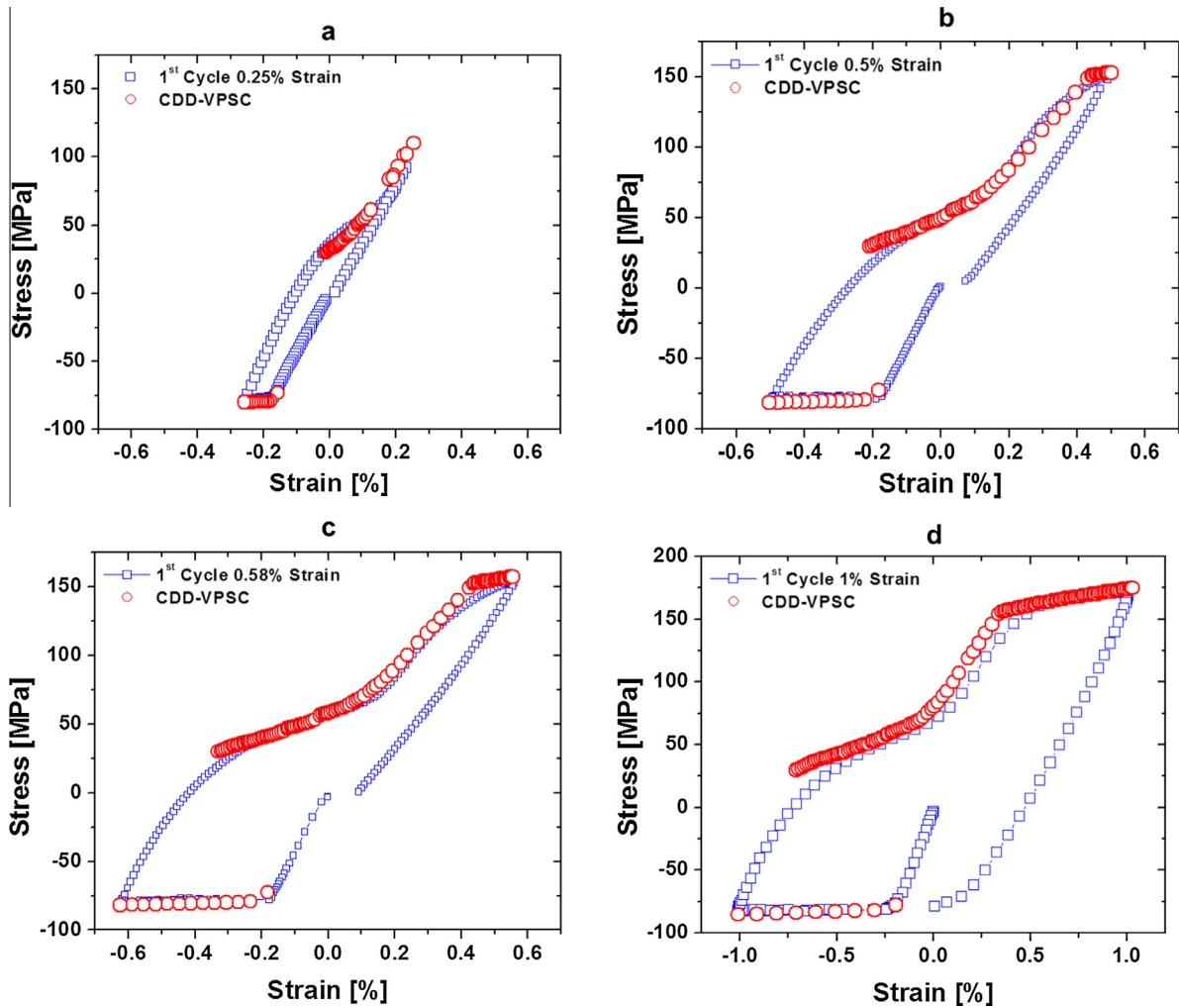


**Fig. 15.** Measured and predicted stress–strain curve under fatigue (compression–tension): first cycle for (a) 0.25% (b) 0.5% (c) 0.58% and (d) 1% applied cyclic strain amplitudes.

The modeling results shown in Fig. 15 demonstrate the key role of imposed cyclic strain on the shape of the modeled stress–strain curves. For smaller values of imposed strain amplitude, only weak twinning conditions are created which could practically lead to relatively small twinned regions that quickly vanish due to detwinning after the loading direction reverses. In fact, detwinning is the major reason for the observed pseudoelasticity in the unloading stage. Note that the nucleation-less nature of detwinning could be viewed as the physical reason behind the assumption of relatively small CRSS for initiation of detwinning (10 MPa) compared to the larger CRSS required for twinning (38 MPa). The “s-type” behavior marked by an inflection point at early stages of tensile loading is not observed for the small strain amplitude (Fig. 15a), while a rapid hardening response due to activation of non-basal systems other than twinning is observed for the larger strain amplitudes. Conversely, twinning in compression is active over a longer extent of plastic deformation for the larger strain amplitudes, which leads to thickening of the twinned regions. This could further lead to the presence of small twinned areas alongside the well-defined larger twinned regions. These small twins are very unstable and thus can detwin as soon as unloading starts. The larger twinned regions, however, provide enough volume fractions for the detwinning mechanism to “consume” and thereby a well-defined plateau associated with the detwinning activity is observed.

The role of twinning–detwinning is also important in regards to the differences observed between the mechanical response in the first and second fatigue cycle. Generally the second cycle is characterized by an extended plateau region before significant hardening is observed at early tensile loading stages since the twinning mechanism is expected to be activated for a longer period in the preceding compressive stage in the first cycle, as also described by Wang et al. (2013). Fig. 16 shows the results of the simulation for the first and second cycle for strain amplitude of 0.5%. The extended plateau as a consequence of detwinning is due to retardation of the hardening response, because more twinning activity has been stored in the previous compression stage of the first cycle.

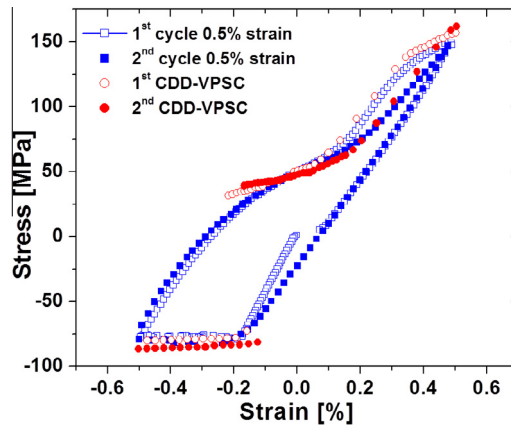


Fig. 16. Comparison of experimental and modeling results for the first and second cycle (Strain amplitude of 0.5%).

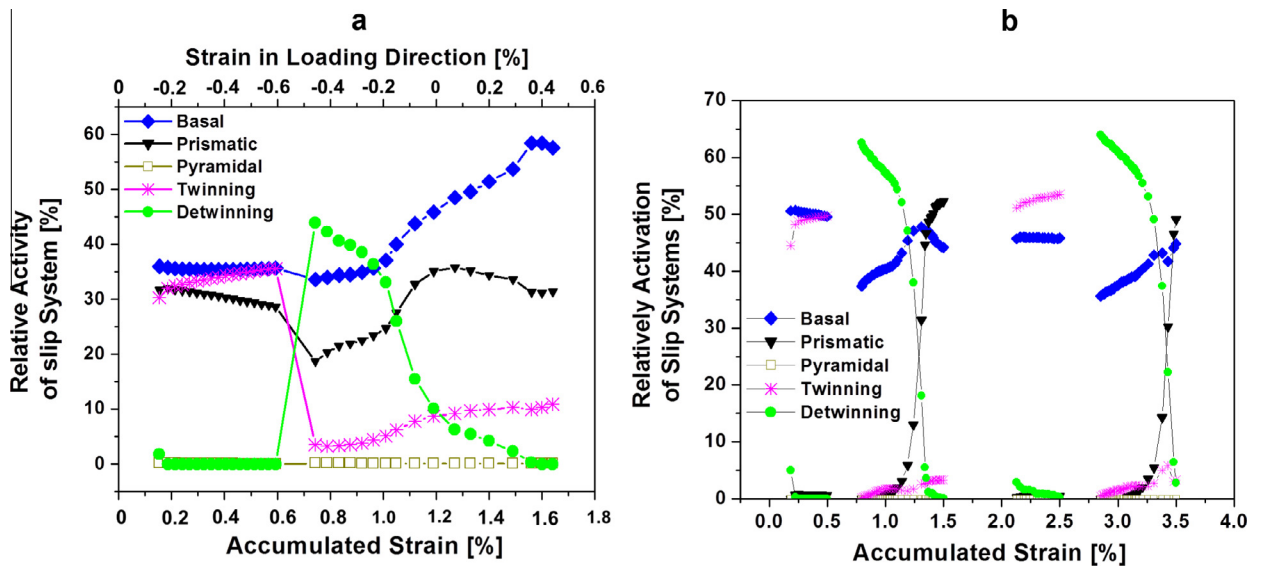


Fig. 17. Relative activity of various deformation mechanisms during cyclic compression–tension loading in (a) first cycle (b) first and second cycle combined.

In Fig. 17a and b the details of the active deformation mechanisms in the first cycle and first and second cycle together for strain amplitude of 0.5% are displayed, respectively. In this diagram, the relative activities of various deformation systems are calculated as shear rates in each deformation system divided by the total shear rate at each time step and averaged over all grains. The modeling results show that twinning and basal slip are the most active mechanisms in the compression stage which causes the formation of twinned areas in the grains. Upon load reversal these twinned regions undergo detwinning starting by smaller unstable twins and continuing to larger twinned areas until the twin volume fraction decreases almost to zero. At this stage, non-basal dislocation mechanisms become more active and the stress–strain curve shows a transition from the detwinning plateau to a steep hardening curve, arising from the dislocation activities as displayed in Fig. 17. Since detwinning is retraction of the existing twins, it does not include hardening effect. In fact, since detwinning causes reduction in twin volume fraction, easier dislocation glide should be expected. But as soon as the activity of the dislocation systems pick up in the activity plot, a hardening response should be expected due to dislocation multiplications and interactions arising from slip. The complete exhaustion of detwinning mechanism leads to behavior similar to the tensile curve presented in Fig. 2 for tension results. In the second cycle the twinning activity has the largest participation in the plastic deformation during compression. This process collectively leads to storage of more twins in the polycrystal. Naturally presence of more twinned regions allows more activity of the detwinning mechanism upon load reversal. Therefore, in the following tension stage of the second cycle, detwinning is more active and hard non-basal systems show less activity, causing a decrease in the stress levels in the tension stage of second cycle as shown in Fig. 14b.

3.6. Energy-based fatigue life prediction

A strain-based approach is generally used to characterize LCF behavior. This approach considers the plastic deformation that often occurs in localized regions where cracks nucleate (Roessle and Fatemi, 2000). In LCF, the plastic strain amplitude is a quantity that has been related to the initiation of several damage processes, while it also influences the microstructure in a way that eventually also affects strain resistance and fatigue life. The plastic strain energy density per cycle is regarded as a critical fatigue damage parameter, because it is comprised of plastic straining due to the activation of deformation mechanisms and their resistance against their motion (Morrow, 1965). Therefore, energy-based fatigue parameters, e.g. in Morrow’s model have been adopted to incorporate the dissipation of strain energy, which occurs as a localized phenomenon at the scale of the material microstructure. This approach has been used to predict the fatigue life for wide range of materials including Mg based alloys (Begum et al., 2009). Specifically, Morrow’s model which relates the number of cycles to failure to plastic strain energy is given as

$$\Delta W_p \cdot N_f^m = C \tag{10}$$

where  $\Delta W_p$ ,  $N_f$  and  $C$  represent plastic strain energy (shown in Fig. 4), fatigue life at half-life and a material constant (depending on fatigue exponent and material energy absorption capacity), respectively. It should be noted, however, that the effect of mean stress which is known to be an important parameters on the fatigue resistance (Kujawski and Ellyin, 1995), is not regarded in Morrow’s model mean stress evolution as a function of fatigue life in Mg alloy is presented in Fig. 7c. To account for this, Ellyin and Kujawski (Ellyin and Kujawski, 1993) incorporated the mean stress effect into a model discussed in Eq. (11), as

$$\Delta W_t \cdot N_f^m = C \tag{11}$$

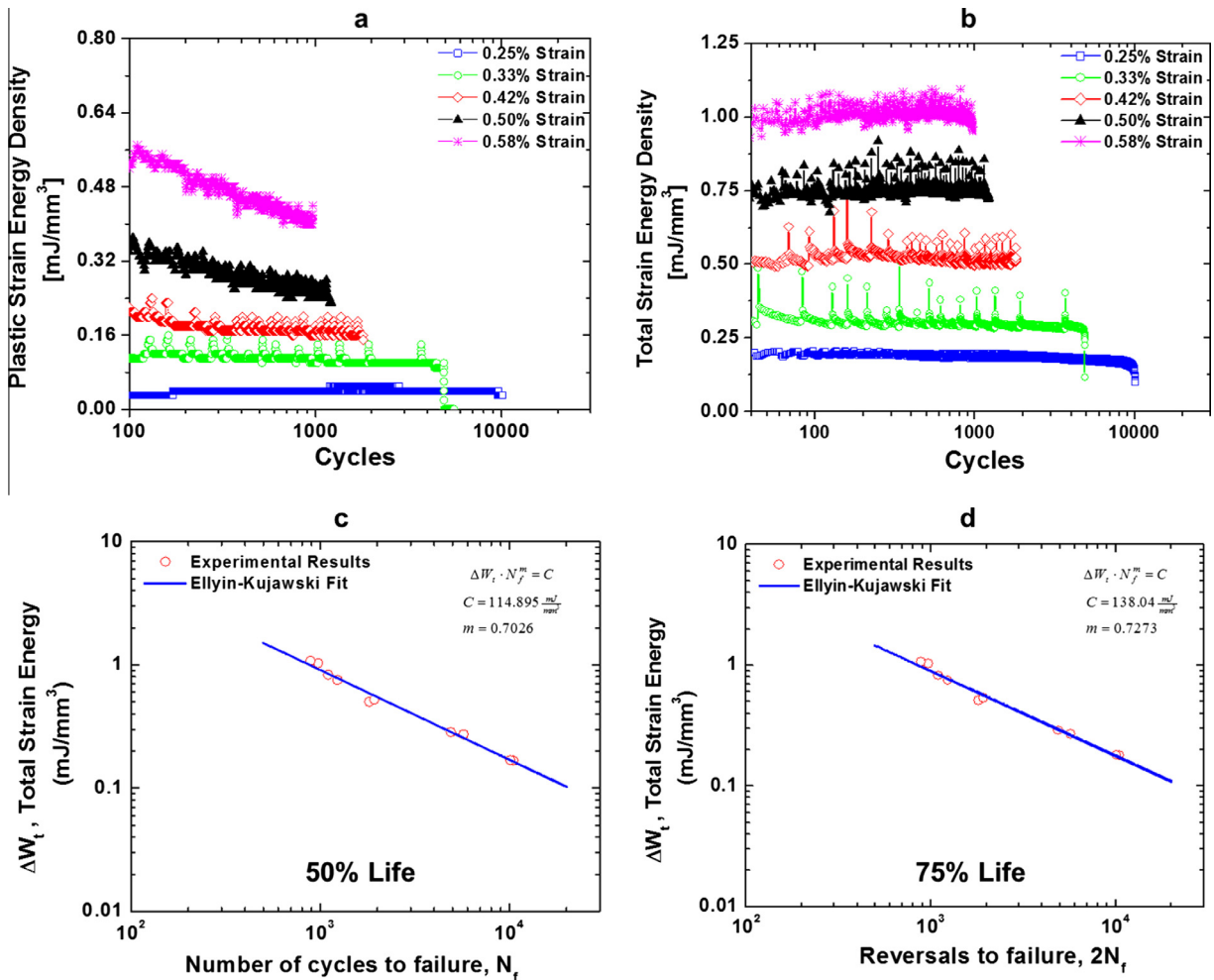


Fig. 18. (a) Plastic and (b) total strain energy density evolution as a function of number of cycles to failure. Fatigue life prediction with the energy based model according to the (c) half-life criteria (d) third-quarter life criteria.

where  $\Delta W_t = (\Delta W_p + \Delta W_e)$  represents the total strain energy at half-life (see Fig. 4). Fig. 18a and b shows total fatigue life (in cycles) predicted by this model as a function of plastic and total strain energy density, for several applied strain amplitudes. It can be observed that the plastic strain energy swiftly decreases for the samples tested using the larger strain amplitude values, while for strain amplitudes equal to 0.25% and 0.33% the plastic strain energy remained fairly constant.

It is, however, important to note that by introducing the (positive) elastic energy (shown in Fig. 4) a criterion over the fatigue life can be obtained. This trend is given in Fig. 18b and as a correlation between the total energy and fatigue life prediction in Fig. 18c and d. The results presented in Fig. 18a and b together with the evolution of mean stress shown in Fig. 7c demonstrate the high sensitivity of the fatigue life to the mean stress especially at higher levels of strain amplitude. This also suggests that the Coffin–Manson approach would not yield an accurate life prediction in strain-control fatigue and especially for high strain amplitudes, since the effect of mean stress is not included. Fig. 18c shows the comparison of the experimental data and the prediction for half-life, whereas Fig. 18d corresponds to the third-quarter life prediction. This comparison shows only insignificant differences between the model predictions for half-life and quarter-life. Since the energy-based approach relies on the collective effect of localized changes it can successfully comprise volumetric effects which cannot be viewed on the surface, and therefore serves as a macroscopic estimation approach based on the procedure followed in this article.

#### 4. Concluding remarks

A systematic experimental approach comprising a parametric investigation of the effect that imposed strain has on the low cycle fatigue behavior of Mg alloys was combined with targeted microstructural observations throughout the fatigue life, and with both crystal plasticity modeling and total life predictions. The dominant role of twinning–detwinning in localized plasticity and damage incubation of Mg alloys was examined in relation to direct observation of surface morphology, texture effects, and nondestructive monitoring. Results for the first fatigue cycle were analyzed in conjunction with subsequent cycles, including the half and three-quarters of total life. The evolution of twinning and surface morphology as a function of fatigue cycles provided strong evidence that they are related to the development of damage-prone areas from which microcracks were shown to originate. Accompanying continuum dislocation dynamics crystal plasticity modeling in a viscoplastic self-consistent scheme was successful in incorporating important experimental information while it further assisted the explanation of the role of detwinning and slip in the hardening behavior. These results were further paired with energy-based fatigue life predictions that by taking into account mean stress effects were capable to provide life estimates based on the obtained experimental fatigue data.

#### Acknowledgments

The corresponding author would like to thank National Science Foundation (NSF) for the financial support provided through the CMMI #1434506 award to Drexel University. The modeling effort in this publication by authors Askari and Zbib was made possible by a National Priorities Research Program grant from the Qatar National Research Fund (a member of The Qatar Foundation), Grant number NPRP 09-611-2-236. Authors Carpick and Streller acknowledge financial support from the NSF under grant CMMI #1334241. In addition author Hazeli would like to thank B Anasori and D. Christe for their kind assistance in data collection and post processing. The extensive support of the Department of Mechanical Engineering and Mechanics and Drexel's Centralized Research Facilities (CRF) is also acknowledged.

#### References

- Abuzaid, W., Sehittoglu, H., Lambros, J., 2013. Plastic strain localization and fatigue micro-crack formation in Hastelloy X. *Mater. Sci. Eng., A* 561, 507–519.
- Agnew, S.R., Duygulu, O., 2005. Plastic anisotropy and the role of non-basal slip in magnesium alloy AZ31B. *Int. J. Plast.* 21, 1161–1193.
- Al-Maharbi, M., Karaman, I., Beyerlein, I.J., Foley, D., Hartwig, K.T., Kecskes, L.J., Mathaudhu, S.N., 2011. Microstructure, crystallographic texture, and plastic anisotropy evolution in an Mg alloy during equal channel angular extrusion processing. *Mater. Sci. Eng., A* 528, 7616–7627.
- Ando, D., Koike, J., Sutou, Y., 2010. Relationship between deformation twinning and surface step formation in AZ31 magnesium alloys. *Acta Mater.* 58, 4316–4324.
- Antolovich, S.D., Armstrong, R.W., 2014. Plastic strain localization in metals: origins and consequences. *Prog. Mater. Sci.* 59, 1–160.
- Askari, H., Young, J., Field, D., Kridli, G., Li, D., Zbib, H., 2014. A study of the hot and cold deformation of twin-roll cast magnesium alloy AZ31. *Phil. Mag.* 94 (4), 381–403.
- Barnett, M., 2001. Influence of deformation conditions and texture on the high temperature flow stress of magnesium AZ31. *J. Light Met.* 1, 167–177.
- Barnett, M., 2007. Twinning and the ductility of magnesium alloys: Part I: “Tension” twins. *Mater. Sci. Eng., A* 464, 1–7.
- Barnett, M.R., Nave, M.D., Bettles, C.J., 2004. Deformation microstructures and textures of some cold rolled Mg alloys. *Mater. Sci. Eng. A (Struct. Mater.: Propert., Microstruct. Process.)* A386, 205–211.
- Barnett, M.R., Nave, M.D., Ghaderi, A., 2012. Yield point elongation due to twinning in a magnesium alloy. *Acta Mater.* 60, 1433–1443.
- Basinski, Z., Pascual, R., Basinski, S., 1983. Low amplitude fatigue of copper single crystals—I. The role of the surface in fatigue failure. *Acta Metall.* 31, 591–602.
- Begum, S., Chen, D., Xu, S., Luo, A.A., 2009. Low cycle fatigue properties of an extruded AZ31 magnesium alloy. *Int. J. Fatigue* 31, 726–735.
- Beyerlein, I., Capolungo, L., Marshall, P., McCabe, R., Tomé, C., 2010. Statistical analyses of deformation twinning in magnesium. *Phil. Mag.* 90, 2161–2190.
- Brahme, A.P., Inal, K., Mishra, R.K., Saimoto, S., 2011. The backstress effect of evolving deformation boundaries in FCC polycrystals. *Int. J. Plast.* 27, 1252–1266.
- Brooks, C.R., Choudhury, A., 2002. *Failure analysis of engineering materials*. McGraw-Hill, New York.
- Caceres, C., Sumitomo, T., Veidt, M., 2003. Pseudoelastic behaviour of cast magnesium AZ91 alloy under cyclic loading–unloading. *Acta Mater.* 51, 6211–6218.
- Chan, K.S., 2010. Roles of microstructure in fatigue crack initiation. *Int. J. Fatigue* 32, 1428–1447.

- Eisenmeier, G., Holzwarth, B., Höppel, H.W., Mughrabi, H., 2001. Cyclic deformation and fatigue behaviour of the magnesium alloy AZ91. *Mater. Sci. Eng., A* 319–321, 578–582.
- Ellyin, F., Kujawski, D., 1993. A multiaxial fatigue criterion including mean-stress effect. *ASTM Spec. Tech. Publ.* 1191, 55–55.
- Eshelby, J.D., 1957. The determination of the elastic field of an ellipsoidal inclusion, and related problems. *Proc. Roy. Soc. Lond. Ser. A, Math. Phys. Sci.* 241, 376–396.
- Ewing, J., Humfrey, J., 1903. The fracture of metals under repeated alternations of stress. *Phil. Trans. Roy. Soc. Lond. Ser. A, Contain. Pap. Math. Phys. Charact.* 200, 241–250.
- Fan, C.L., Chen, D.L., Luo, A.A., 2009. Dependence of the distribution of deformation twins on strain amplitudes in an extruded magnesium alloy after cyclic deformation. *Mater. Sci. Eng., A* 519, 38–45.
- Finney, J., Laird, C., 1975. Strain localization in cyclic deformation of copper single crystals. *Phil. Mag.* 31, 339–366.
- Geng, C.J., Wu, B.L., Du, X.H., Wang, Y.D., Zhang, Y.D., Wagner, F., Esling, C., 2013. Low cycle fatigue behavior of the textured AZ31B magnesium alloy under the asymmetrical loading. *Mater. Sci. Eng., A* 560, 618–626.
- Harvey, S., Marsh, P., Gerberich, W., 1994. Atomic force microscopy and modeling of fatigue crack initiation in metals. *Acta Metall. Mater.* 42, 3493–3502.
- Hasegawa, S., Tsuchida, Y., Yano, H., Matsui, M., 2007. Evaluation of low cycle fatigue life in AZ31 magnesium alloy. *Int. J. Fatigue* 29, 1839–1845.
- Hazeli, K., Cuadra, J., Vanniamparambil, P.A., Kontsos, A., 2013a. In situ identification of twin-related bands near yielding in a magnesium alloy. *Scripta Mater.* 68, 83–86.
- Hazeli, K., Sadeghi, A., Pekguleryuz, M.O., Kontsos, A., 2013b. The effect of strontium in plasticity of magnesium alloys. *Mater. Sci. Eng., A* 578, 383–393.
- Hazeli, K., Cuadra, J., Streller, F., Barr, C.M., Carpick, R.W., Taheri, M.L., Kontsos, A., 2014. 3D surface effects of twinning in magnesium alloys. *Scripta Mater.*, accepted for publication.
- Hull, D., 1999. *Fractography: Observing, Measuring and Interpreting Fracture Surface Topography*. Cambridge University Press.
- Hyuk Park, S., Hong, S.-G., Ho Lee, B., Bang, W., Soo Lee, C., 2010. Low-cycle fatigue characteristics of rolled Mg–3Al–1Zn alloy. *Int. J. Fatigue* 32, 1835–1842.
- Ishihara, S., Nan, Z., Goshima, T., 2007. Effect of microstructure on fatigue behavior of AZ31 magnesium alloy. *Mater. Sci. Eng., A* 468–470, 214–222.
- Jiang, L., Jonas, J., Mishra, R., Luo, A., Sachdev, A., Godet, S., 2007. Twinning and texture development in two Mg alloys subjected to loading along three different strain paths. *Acta Mater.* 55, 3899–3910.
- John Neil, C., Agnew, S.R., 2009. Crystal plasticity-based forming limit prediction for non-cubic metals: application to Mg alloy AZ31B. *Int. J. Plast.* 25, 379–398.
- Jordon, J., Gibson, J., Horstemeyer, M., Kadiri, H.E., Baird, J., Luo, A., 2011. Effect of twinning, slip, and inclusions on the fatigue anisotropy of extrusion-textured AZ61 magnesium alloy. *Mater. Sci. Eng., A* 528, 6860–6871.
- Kabirian, F., Khan, A.S., Pandey, A., 2014. Negative to positive strain rate sensitivity in 5xxx series aluminum alloys: experiment and constitutive modeling. *Int. J. Plast.* 55, 232–246.
- Kalidindi, S.R., 1998. Incorporation of deformation twinning in crystal plasticity models. *J. Mech. Phys. Solids* 46, 267–290.
- Karaman, I., Sehitoglu, H., Chumlyakov, Y.I., Maier, H.J., Kireeva, I., 2001. The effect of twinning and slip on the Bauschinger effect of Hadfield steel single crystals. *Metall. Mater. Trans. A* 32, 695–706.
- Khan, A.S., Pandey, A., Gnäupel-Herold, T., Mishra, R.K., 2011. Mechanical response and texture evolution of AZ31 alloy at large strains for different strain rates and temperatures. *Int. J. Plast.* 27, 688–706.
- Kleiner, S., Uggowitzer, P., 2004. Mechanical anisotropy of extruded Mg–6%Al–1%Zn alloy. *Mater. Sci. Eng., A* 379, 258–263.
- Koike, J., 2005. Enhanced deformation mechanisms by anisotropic plasticity in polycrystalline Mg alloys at room temperature. *Metall. Mater. Trans. A* 36, 1689–1696.
- Koike, J., Fujiyama, N., Ando, D., Sutou, Y., 2010. Roles of deformation twinning and dislocation slip in the fatigue failure mechanism of AZ31 Mg alloys. *Scripta Mater.* 63, 747–750.
- Kujawski, D., Ellyin, F., 1995. A unified approach to mean stress effect on fatigue threshold conditions. *Int. J. Fatigue* 17, 101–106.
- Le Biavant, K., Pommier, S., Prioul, C., 2002. Local texture and fatigue crack initiation in a Ti–6Al–4V titanium alloy. *Fatigue Fract. Eng. Mater. Struct.* 25, 527–545.
- Lebensohn, R., Tomé, C., 1993. A self-consistent anisotropic approach for the simulation of plastic deformation and texture development of polycrystals: application to zirconium alloys. *Acta Metall. Mater.* 41, 2611–2624.
- Li, D., Zbib, H., Sun, X., Khaleel, M., 2013. Predicting plastic flow and irradiation hardening of iron single crystal with mechanism-based continuum dislocation dynamics. *Int. J. Plast.*
- Llanes, L., Rollett, A., Laird, C., Bassani, J., 1993. Effect of grain size and annealing texture on the cyclic response and the substructure evolution of polycrystalline copper. *Acta Metall. Mater.* 41, 2667–2679.
- Lou, X., Li, M., Boger, R., Agnew, S., Wagoner, R., 2007. Hardening evolution of AZ31B Mg sheet. *Int. J. Plast.* 23, 44–86.
- Lu, Y., Gharghour, M., Taheri, F., 2008. Effect of texture on acoustic emission produced by slip and twinning in AZ31B magnesium alloy—part II: clustering and neural network analysis. *Nondestruct. Test. Eval.* 23, 211–228.
- Lugo, M., Jordon, J., Solanki, K., Hector Jr, L., Bernard, J., Luo, A., Horstemeyer, M., 2013. Role of different material processing methods on the fatigue behavior of AZ31 magnesium alloy. *Int. J. Fatigue*.
- Lv, F., Yang, F., Duan, Q.Q., Luo, T.J., Yang, Y.S., Li, S.X., Zhang, Z.F., 2009. Tensile and low-cycle fatigue properties of Mg–2.8%Al–1.1.%Zn–0.4%Mn alloy along the transverse and rolling directions. *Scripta Mater.* 61, 887–890.
- Lv, F., Yang, F., Duan, Q., Yang, Y., Wu, S., Li, S., Zhang, Z., 2011. Fatigue properties of rolled magnesium alloy (AZ31) sheet: influence of specimen orientation. *Int. J. Fatigue* 33, 672–682.
- Man, J., Vystavěl, T., Weidner, A., Kuběna, I., Petrevec, M., Kruml, T., Polák, J., 2012. Study of cyclic strain localization and fatigue crack initiation using FIB technique. *Int. J. Fatigue* 39, 44–53.
- Matsuzuki, M., Horibe, M., 2009. Analysis of fatigue damage process in magnesium alloy AZ31. *Mater. Sci. Eng., A* 504, 169–174.
- McDowell, D.L., 2007. Simulation-based strategies for microstructure-sensitive fatigue modeling. *Mater. Sci. Eng., A* 468, 4–14.
- McDowell, D.L., Dunne, F.P.E., 2010. Microstructure-sensitive computational modeling of fatigue crack formation. *Int. J. Fatigue* 32, 1521–1542.
- Morrison, D.J., Moosbrugger, J.C., 1997. Effects of grain size on cyclic plasticity and fatigue crack initiation in nickel. *Int. J. Fatigue* 19, 51–59.
- Morrow, J., 1965. *Cyclic Plastic Strain Energy and Fatigue of Metals*. ASTM STP 378, American Society for Testing and Materials, Philadelphia, PA, pp. 45–84.
- Mughrabi, H., Herz, K., Stark, X., 1981. Cyclic deformation and fatigue behaviour of  $\alpha$ -iron mono- and polycrystals. *Int. J. Fract.* 17, 193–220.
- Muránsky, O., Barnett, M., Carr, D., Vogel, S., Oliver, E., 2010. Investigation of deformation twinning in a fine-grained and coarse-grained ZM20 Mg alloy: combined *in situ* neutron diffraction and acoustic emission. *Acta Mater.* 58, 1503–1517.
- Ohashi, T., Kawamukai, M., Zbib, H., 2007. A multiscale approach for modeling scale-dependent yield stress in polycrystalline metals. *Int. J. Plast.* 23, 897–914.
- Oppedal, A.L., El Kadiri, H., Tomé, C.N., Kaschner, G.C., Vogel, S.C., Baird, J.C., Horstemeyer, M.F., 2012. Effect of dislocation transmutation on modeling hardening mechanisms by twinning in magnesium. *Int. J. Plast.* 30–31, 41–61.
- Park, S.H., Hong, S.-G., Bang, W., Lee, C.S., 2010a. Effect of anisotropy on the low-cycle fatigue behavior of rolled AZ31 magnesium alloy. *Mater. Sci. Eng., A* 527, 417–423.
- Park, S.H., Hong, S.-G., Lee, C.S., 2010b. Activation mode dependent 10–12 twinning characteristics in a polycrystalline magnesium alloy. *Scripta Mater.* 62, 202–205.
- Partridge, P., 1965. Cyclic twinning in fatigued close-packed hexagonal metals. *Phil. Mag.* 12, 1043–1054.
- Peralta, P., Choi, S.H., Gee, J., 2007. Experimental quantification of the plastic blunting process for stage II fatigue crack growth in one-phase metallic materials. *Int. J. Plast.* 23, 1763–1795.

- Pham, M.S., Holdsworth, S.R., Janssens, K.G.F., Mazza, E., 2013. Cyclic deformation response of AISI 316L at room temperature: mechanical behaviour, microstructural evolution, physically-based evolutionary constitutive modelling. *Int. J. Plast.* 47, 143–164.
- Proust, G., Tomé, C.N., Jain, A., Agnew, S.R., 2009. Modeling the effect of twinning and detwinning during strain-path changes of magnesium alloy AZ31. *Int. J. Plast.* 25, 861–880.
- Raesisinia, B., Agnew, S.R., Akhtar, A., 2011. Incorporation of solid solution alloying effects into polycrystal modeling of Mg alloys. *Metall. Mater. Trans. A* 42, 1418–1430.
- Ritchie, R., Suresh, S., 1982. Some considerations on fatigue crack closure at near-threshold stress intensities due to fracture surface morphology. *Metall. Trans. A* 13, 937–940.
- Robson, J., Stanford, N., Barnett, M., 2011. Effect of precipitate shape on slip and twinning in magnesium alloys. *Acta Mater.* 59, 1945–1956.
- Roessle, M.L., Fatemi, A., 2000. Strain-controlled fatigue properties of steels and some simple approximations. *Int. J. Fatigue* 22, 495–511.
- Shan, Z., Gokhale, A.M., 2004. Digital image analysis and microstructure modeling tools for microstructure sensitive design of materials. *Int. J. Plast.* 20, 1347–1370.
- Suresh, S., 1998. *Fatigue of Materials*. Cambridge University Press.
- Tanaka, K., Mura, T., 1982. A theory of fatigue crack initiation at inclusions. *Metall. Trans. A* 13, 117–123.
- Tome, C., Lebensohn, R., Kocks, U., 1991. A model for texture development dominated by deformation twinning: application to zirconium alloys. *Acta Metall. Mater.* 39, 2667–2680.
- Tomé, C., Lebensohn, R., Kocks, U., 1991. A model for texture development dominated by deformation twinning: application to zirconium alloys. *Acta Metall. Mater.* 39, 2667–2680.
- Trager-Cowan, C., Sweeney, F., Trimby, P., Day, A., Gholinia, A., Schmidt, N.-H., Parbrook, P., Wilkinson, A., Watson, I., 2007. Electron backscatter diffraction and electron channeling contrast imaging of tilt and dislocations in nitride thin films. *Phys. Rev. B* 75, 085301.
- Vaidya, S., Mahajan, S., 1980. Accommodation and formation of 1121 twins in Co single crystals. *Acta Metall.* 28, 1123–1131.
- Venkataraman, G., Chung, Y., Mura, T., 1991. Application of minimum energy formalism in a multiple slip band model for fatigue—I. Calculation of slip band spacings. *Acta Metall. Mater.* 39, 2621–2629.
- Voce, E., 1955. A practical strain-hardening function. *Metallurgia* 51, 219–226.
- Wang, Y., Huang, J., 2007. The role of twinning and untwinning in yielding behavior in hot-extruded Mg–Al–Zn alloy. *Acta Mater.* 55, 897–905.
- Wang, H., Raesisinia, B., Wu, P., Agnew, S., Tomé, C., 2010a. Evaluation of self-consistent polycrystal plasticity models for magnesium alloy AZ31B sheet. *Int. J. Solids Struct.* 47, 2905–2917.
- Wang, H., Wu, Y., Wu, P., Neale, K., 2010b. Numerical analysis of large strain simple shear and fixed-end torsion of HCP polycrystals. *Comp. Mater. Cont.* 19, 255.
- Wang, H., Berdin, C., Mazzière, M., Forest, S., Prioul, C., Parrot, A., Le-Delliou, P., 2011. Portevin–Le Chatelier (PLC) instabilities and slant fracture in C–Mn steel round tensile specimens. *Scripta Mater.* 64, 430–433.
- Wang, H., Wu, P., Tomé, C., Wang, J., 2012. A constitutive model of twinning and detwinning for hexagonal close packed polycrystals. *Mater. Sci. Eng., A* 555, 93–98.
- Wang, H., Wu, P., Wang, J., Tomé, C., 2013. A crystal plasticity model for hexagonal close packed (HCP) crystals including twinning and de-twinning mechanisms. *Int. J. Plast.*
- Wei, Q., Cheng, S., Ramesh, K.T., Ma, E., 2004. Effect of nanocrystalline and ultrafine grain sizes on the strain rate sensitivity and activation volume: fcc versus bcc metals. *Mater. Sci. Eng., A* 381, 71–79.
- Wu, L., Agnew, S., Brown, D., Stoica, G., Clausen, B., Jain, A., Fielden, D., Liaw, P., 2008a. Internal stress relaxation and load redistribution during the twinning–detwinning-dominated cyclic deformation of a wrought magnesium alloy, ZK60A. *Acta Mater.* 56, 3699–3707.
- Wu, L., Jain, A., Brown, D., Stoica, G., Agnew, S., Clausen, B., Fielden, D., Liaw, P., 2008b. Twinning–detwinning behavior during the strain-controlled low-cycle fatigue testing of a wrought magnesium alloy, ZK60A. *Acta Mater.* 56, 688–695.
- Wu, L., Jain, A., Brown, D.W., Stoica, G.M., Agnew, S.R., Clausen, B., Fielden, D.E., Liaw, P.K., 2008c. Twinning–detwinning behavior during the strain-controlled low-cycle fatigue testing of a wrought magnesium alloy, ZK60A. *Acta Mater.*
- Wu, L., Agnew, S.R., Ren, Y., Brown, D.W., Clausen, B., Stoica, G.M., Wenk, H.R., Liaw, P.K., 2010. The effects of texture and extension twinning on the low-cycle fatigue behavior of a rolled magnesium alloy AZ31B.
- Yang, F., Yin, S., Li, S., Zhang, Z., 2008. Crack initiation mechanism of extruded AZ31 magnesium alloy in the very high cycle fatigue regime. *Mater. Sci. Eng., A* 491, 131–136.
- Yang, F., Lv, F., Yang, X., Li, S., Zhang, Z., Wang, Q., 2011. Enhanced very high cycle fatigue performance of extruded Mg–12Gd–3Y–0.5Zr magnesium alloy. *Mater. Sci. Eng., A* 528, 2231–2238.
- Yin, S.M., Yang, F., Yang, X.M., Wu, S.D., Li, S.X., Li, G.Y., 2008a. The role of twinning–detwinning on fatigue fracture morphology of Mg–3%Al–1%Zn alloy. *Mater. Sci. Eng., A* 494, 397–400.
- Yin, S.M., Yang, H.J., Li, S.X., Wu, S.D., Yang, F., 2008b. Cyclic deformation behavior of as-extruded Mg–3%Al–1%Zn. *Scripta Mater.* 58, 751–754.
- Yoo, M., 1981. Slip, twinning, and fracture in hexagonal close-packed metals. *Metall. Trans. A* 12, 409–418.
- Zeng, R., Han, E., Ke, W., Dietzel, W., Kainer, K.U., Atrens, A., 2010. Influence of microstructure on tensile properties and fatigue crack growth in extruded magnesium alloy AM60. *Int. J. Fatigue* 32, 411–419.
- Zhang, J., Jiang, Y., 2006. Fatigue of polycrystalline copper with different grain sizes and texture. *Int. J. Plast.* 22, 536–556.
- Zhang, J., Yu, Q., Jiang, Y., Li, Q., 2011. An experimental study of cyclic deformation of extruded AZ61A magnesium alloy. *Int. J. Plast.* 27, 768–787.